



Executive summary

Wind turbine noise: primary noise sources

Problem area

Wind is a clean, cheap, and inexhaustible source of energy. However, the noise from wind turbines constitutes an important hindrance for the widespread application of wind energy. As a result, there is considerable interest in wind turbine noise, from a number of angles. As public clamour grows from those living near turbines, and misinformation and disinformation begin to take root, there is a clear need for a scientifically accurate book to give an account of the noise generated, its effects on people, and possible remedies either through technology or legislation or both.

Description of work

This report constitutes the chapter "Primary Noise Sources" of the book "Wind Turbine Noise", to be published by MultiScience in 2011. The different potential source mechanisms are described and the theoretical characteristics of flow-induced sound from wind turbine blades are explained. The noise sources on wind turbines are characterized experimentally by

means of wind tunnel and field experiments. Methods to predict and reduce wind turbine noise are discussed.

Results and conclusions

The dominant noise source for typical modern large wind turbines is broadband trailing edge noise from the outer part of the blades. The swishing character of the sound can be explained by trailing edge noise directivity and convective amplification. A semi-analytical, semi-empirical prediction method can accurately predict the characteristics of wind turbine noise. Wind turbine noise can be halved by means of serrations, without adverse effects on the aerodynamic performance.

Applicability

The book is aimed at people with a personal or professional involvement in wind turbine noise, such as environmental health or public health practitioners, wind farm developers or informed wind farm supporters and objectors.

Report no.

NLR-TP-2011-066

Author(s)

S. Oerlemans

Report classification

UNCLASSIFIED

Date

April 2011

Knowledge area(s)

Aeroacoustic and experimental aerodynamic research

Descriptor(s)

wind turbines
aerodynamic noise

This report is based on the chapter "Primary noise sources" of the book "Wind Turbine Noise", to be published by MultiScience in 2011.



NLR-TP-2011-066

Wind turbine noise: primary noise sources

S. Oerlemans




This report is based on the chapter "Primary noise sources" of the book "Wind Turbine Noise", to be published by MultiScience in 2011.

The contents of this report may be cited on condition that full credit is given to NLR and the authors.

This publication has been refereed by the Advisory Committee AEROSPACE VEHICLES.

Customer	MultiScience
Contract number	----
Owner	National Aerospace Laboratory NLR
Division NLR	Aerospace Vehicles
Distribution	Unlimited
Classification of title	Unclassified
	April 2011

Approved by:

Author	Reviewer	Managing department
 15/4/11	 18/4/11	

Summary

This report addresses the primary sources of wind turbine noise. First, the different potential source mechanisms are described and the theoretical characteristics of flow-induced sound from wind turbine blades are explained. It is shown that the sound power scales with at least the 5th power of the flow speed, and that the directivity is generally not uniform. Then, the noise sources on wind turbines are characterized experimentally by means of acoustic array measurements in the field. The test results indicate that the dominant noise source for typical modern large wind turbines is broadband trailing edge noise from the outer part of the blades. The swishing character of the sound can be explained by trailing edge noise directivity and convective amplification: each time a blade moves towards the observer, a higher sound level is perceived. Next, it is shown that a semi-analytical, semi-empirical prediction method can accurately predict the characteristics of wind turbine noise. Good agreement is found between predictions and experiment, not only in terms of sound levels and spectra, but also with regard to swish and turbine noise directivity. Calculated noise footprints show that swish amplitudes up to 5 dB can be expected for cross-wind directions, even at large distance. Finally, different noise reduction concepts are described and two of them, an optimized airfoil shape and trailing edge serrations, are tested on a full-scale turbine. Both blade modifications yield a significant trailing edge noise reduction at low frequencies, but also exhibit increased tip noise at high frequencies. Nevertheless, the experimental results show that wind turbine noise can be halved by means of serrations, without adverse effects on the aerodynamic performance. In future, even larger reductions may be achieved using flexible trailing edge brushes.

Contents

1	Preface	5
2	Introduction	5
3	Potential sources of wind turbine noise	6
3.1	Flow around a wind turbine blade	6
3.2	Aerodynamic noise sources	9
4	Characteristics of airfoil noise	11
4.1	Interaction between turbulence and an airfoil surface	11
4.2	Theoretical relations for trailing edge noise	12
4.3	Measurements of trailing edge noise from two-dimensional airfoils	15
4.4	Blunt trailing edge noise	18
4.5	Inflow turbulence noise	19
4.6	Tip noise	21
4.7	Moving sources	21
5	Field measurements of wind turbine noise	22
5.1	Single-microphone measurements	22
5.2	Noise source distribution in the rotor plane	25
5.3	Noise sources on the blades	29
6	Prediction of wind turbine noise	30
6.1	Prediction method	31
6.2	Validation against experiment	32
6.3	Prediction of noise and swish footprints	36
7	Reduction of wind turbine noise	37
7.1	Reduction concepts	38
7.2	Assessment of noise reduction concepts on a full-scale wind turbine	40
8	Conclusion	44
	References	46
Appendix A	Detection of sound sources using phased microphone arrays	49

1 Preface

Wind is a clean, cheap, and inexhaustible source of energy. However, the noise from wind turbines constitutes an important hindrance for the widespread application of wind energy. A recent survey in the Netherlands [1] showed that sound was the most annoying aspect of wind turbines. The swishing character of the noise was mentioned as an important factor explaining the relatively high annoyance, as compared to other sound sources of equal level (air or road traffic). It should be noted that, besides the level and nature of the sound, the perception of noise is significantly influenced by psychological factors. For aircraft noise, it has been shown that annoyance can be reduced substantially by *fair* procedures, even when the actual noise exposure remains the same [2]. Hindrance from wind turbine noise reduces significantly when people have an economic benefit from the turbines [1].

Whatever the reason, long-term exposure to unwanted sounds may cause serious health problems, such as sleep disturbance, reduced concentration, stress or fatigue. In order to protect public health, sound levels in residential areas have to comply with legal regulations. However, these noise limits may constitute a major obstacle for the exploitation of wind energy. Many wind turbines have to operate at reduced power during the night, and in some cases even plans for complete wind farms are cancelled due to noise regulations. For new wind turbines, the size of the blades (and therefore the energy output) is limited by noise constraints.

This report is based on the chapter "Primary noise sources" of the book "Wind Turbine Noise", to be published by MultiScience in 2011. The focus is on large wind turbines, since these are expected to be most relevant for the future of wind energy.

2 Introduction

In order to progress the development of wind power and reduce noise annoyance, it is essential to reduce the sound of wind turbines. However, before we can reduce the sound, we first have to know and understand the *sources* of the noise. This chapter deals with the primary noise sources of modern large wind turbines, and is divided into the following sections:

- Introduction
- Potential sources of wind turbine noise
- Characteristics of airfoil noise
- Field measurements of wind turbine noise
- Prediction of wind turbine noise
- Reduction of wind turbine noise
- Summary

After this introduction we will first discuss the different potential source mechanisms and their characteristics. Then, on the basis of field measurements, we will show that aerodynamic noise from the blades is generally dominant. Moreover, using the characteristics of trailing edge noise, we will be able to understand the swishing character of wind turbine noise. Next, we will show that wind turbine noise can be accurately predicted using a semi-analytical, semi-empirical prediction method, which only needs the blade geometry and operating conditions as input. Finally, we will discuss the possible ways of *reducing* wind turbine noise, and describe validation experiments for different noise reduction concepts.

Throughout this chapter we will see that directional acoustic measurement methods play an important role in experimental wind turbine noise research. This so-called *phased array* technique is explained separately in Appendix 1 at the end of the book. Since we are concerned with *primary* noise sources, we will not consider secondary effects due to sound propagation or wind shear. These effects are addressed in other chapters. The present chapter is mainly based on experience gained at the Dutch National Aerospace Laboratory NLR during the last 10-15 years. As a consequence, most of the examples presented here are taken from projects in which NLR was involved. A limited number of references to relevant work from other groups is given in this chapter. A more complete overview of the available literature can be found in Ref. 3.

3 Potential sources of wind turbine noise

In this chapter we focus on modern large wind turbines, which typically have a horizontal axis and an upwind rotor. The sound from such a turbine can be divided in mechanical noise and aerodynamic noise [4]. Mechanical noise can be generated by different components in the hub, such as the gearbox or the generator, and may contain several tones. However, provided that mechanical noise is adequately treated, aerodynamic noise from the blades is generally the dominant noise source. Therefore, in this section we will briefly discuss the flow around a wind turbine blade, followed by a description of potential aerodynamic source mechanisms.

3.1 Flow around a wind turbine blade

In order to understand the different mechanisms of aerodynamic noise, we first have to look at the air flow around the blade. If we look at a wind turbine from a downwind observer position (i.e., we look in the *upwind* direction), for most modern turbines the blades rotate in anti-clockwise direction (Figure 1). As the upper blade cuts through the air, it experiences an air flow from left to right (Figure 2). As illustrated in Figure 3, the effective flow speed U perceived by the blade is composed of the wind speed U_w and the rotational flow speed U_r . For modern wind turbines, the rotational speed at the blade tip is typically 75 m/s, while the wind speed at rotor height is of the order of 10 m/s. The cross section of the blade (the *airfoil*) is

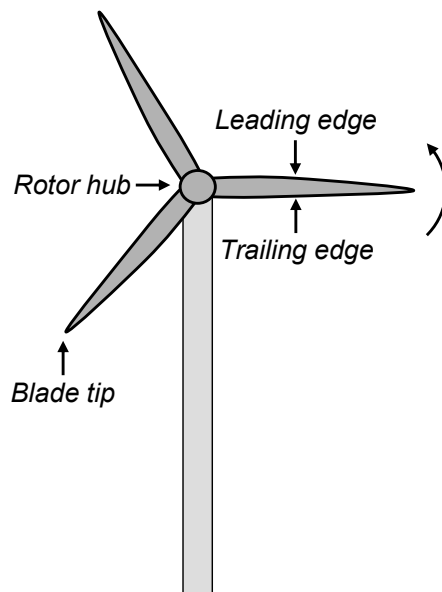


Figure 1 Wind turbine as seen from a downwind position

designed such that it diverts the incoming flow downward (i.e., towards the rotor plane), thus producing a reaction force F . The component of this force in the rotor plane is what makes the rotor blades turn. This is similar to the lift force produced by aircraft wings to keep airplanes in the air. Since the blades divert the flow towards the rotor plane, the rotor effectively slows down the incoming wind, thus extracting energy from it. The lower surface of the airfoil (i.e., the upwind side), where the relatively low flow speed results in a high pressure, is called the *pressure side*. The upper surface, with a high flow speed and low pressure, is called the *suction side*.

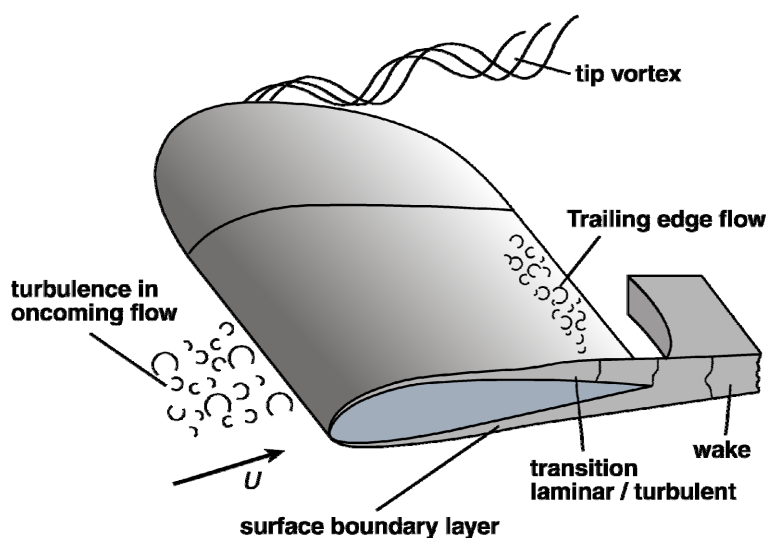


Figure 2 Flow around the outer part of a wind turbine blade [4]

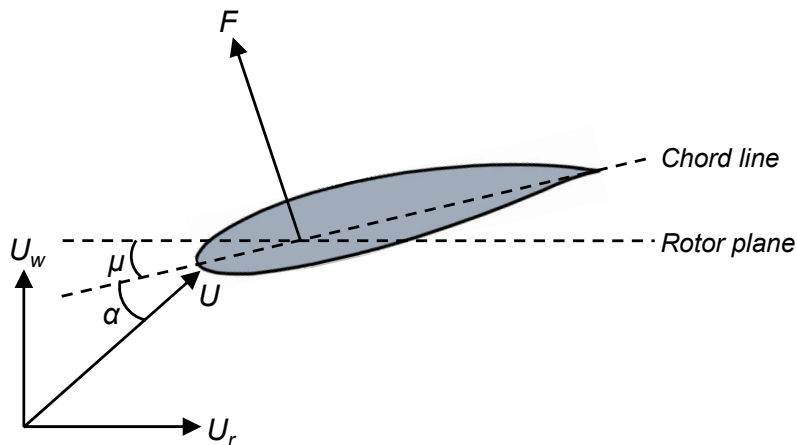


Figure 3 Airfoil with definition of flow angles

The angle between the effective flow direction and the airfoil chord line is called the *angle of attack* α . The angle between the chord line and the rotor plane, μ , is the sum of the (fixed) local blade twist and the (adjustable) blade pitch angle. Thus, Figure 3 illustrates that the angle of attack can be increased by *reducing* the pitch angle. Similarly, a higher wind speed results in an increase in angle of attack. Normally, a higher angle of attack means a higher reaction force F and therefore a higher torque.

As the air flows past the blade, a thin layer of air develops which, due to viscosity, partially 'sticks' to the blade surface (Figure 2). This layer, which is usually less than a few centimetres thick, is called the *boundary layer*. At the blade surface, the air velocity (relative to the blade) is zero, while at the edge of the boundary layer the velocity is equal to the undisturbed flow speed. The structure of the boundary layer depends on the Reynolds number $Re = UC/\nu$, with C the blade chord and ν the kinematic viscosity (about $15 \cdot 10^{-6} \text{ m}^2\text{s}^{-1}$ in air). For the outer part of a large wind turbine blade (where practically all the noise is produced), Re is typically a few millions or more. For these Reynolds numbers, the boundary layer, which is initially laminar, will generally become turbulent somewhere along the chord. Whereas the laminar boundary layer is organized in layers, the turbulent boundary layer is more chaotic and contains turbulent eddies (vortices).

The thickness of the boundary layer can be characterized using $\delta_{0.99}$, the distance from the surface where the mean velocity equals 99% of the undisturbed flow speed. However, this distance is rather ill-defined due to the asymptotic behaviour of the velocity profile at the edge of the boundary layer. Therefore, the thickness of the boundary layer is often characterized using the *displacement thickness* δ^* . This is the distance by which the surface would have to be moved in a hypothetical non-viscous (uniform) flow to maintain the same volumetric flow as in the case with boundary layer. The displacement thickness is typically 1/8 to 1/5 of $\delta_{0.99}$, depending on the shape of the velocity profile. For a turbulent boundary layer over a flat plate, the displacement thickness at distance C from the leading edge can be estimated using the

relation $\delta^*/C \approx 0.05 \text{Re}^{-1/5}$ [5]. For an airfoil, an increase in angle of attack typically results in a thicker boundary layer on the suction side, while the pressure side boundary layer becomes thinner.

3.2 Aerodynamic noise sources

The different aerodynamic noise source mechanisms are illustrated in Figure 2. First, turbulence may be present in the oncoming flow, for example generated by the atmospheric boundary layer or by the wake from upwind turbines in a wind farm. The interaction between the incident eddies and the blade surface may cause *inflow turbulence noise*. This noise source strongly depends on site-specific and time-dependent atmospheric conditions, and it is an open issue to what extent inflow turbulence noise contributes to the overall sound level of a wind turbine. The second source mechanism is related to the tip vortex, which is formed due to the pressure difference between the pressure and suction side of the blade. Turbulence is convected over the tip edge, and separated flow may occur. The interaction between the turbulent flow and the tip surface may cause *tip noise*. This noise source depends on the strength of the tip vortex and on the planform of the blade tip. Finally, noise may be generated by the interaction between the turbulent flow over the 2D airfoil and the trailing edge of the blade. Since this sound, like tip noise, is generated in an undisturbed inflow, it is referred to as airfoil *self noise* [6].

Depending on the flow conditions, several self noise mechanisms may occur (Figure 4). On the outer part of a large wind turbine blade ($\text{Re} > 1$ million), typically a turbulent boundary layer develops along the blade surface, which remains attached up to the trailing edge. As the turbulent eddies are convected past the trailing edge, their sound is scattered at the trailing edge, causing broadband noise. This turbulent-boundary-layer-trailing-edge noise or briefly *trailing edge noise* (Figure 4a) usually defines the lower bound of wind turbine noise, and is considered to be the most important noise source for modern large wind turbines.

If the Reynolds number is smaller than about 1 million, the boundary layer on either side of the airfoil may remain laminar up to the trailing edge. Upstream radiating noise from the trailing edge may then trigger laminar-turbulent transition or boundary layer instabilities (Tollmien-Schlichting waves), which in turn radiate as trailing edge noise. If such a feedback loop occurs, high levels of tonal noise may be generated. This type of whistling noise is called *laminar-boundary-layer-vortex-shedding-noise* (Figure 4b), and can be prevented by tripping the boundary layer, which induces transition from laminar to turbulent flow. This noise source is considered to be only relevant for small wind turbines, which have relatively small blades with Reynolds numbers below 1 million.

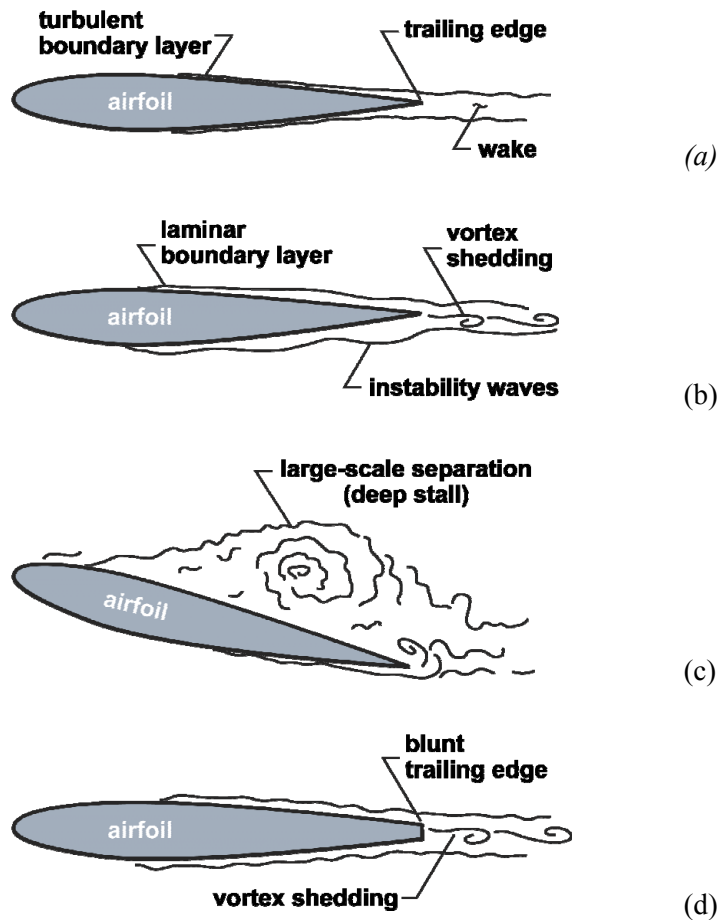


Figure 4 Airfoil self-noise mechanisms [6]

As the angle of attack increases, at some point the flow will separate from the suction side of the airfoil. This corresponds to so-called stall. Stall causes a substantial level of unsteady flow around the airfoil, which may lead to a significant increase in noise [6,7,8,9]. For mildly separated flow this *separation-stall noise* (Figure 4c) appears to be radiated from the trailing edge, whereas deep stall causes low-frequency radiation from the airfoil as a whole. Stall noise is considered to be of minor importance for modern pitch-controlled wind turbines.

Blunt trailing edge noise (Figure 4d) occurs when the trailing edge thickness is increased above a critical value. Periodic Von Karman type vortex shedding from the trailing edge may then result in tonal noise. Normally blunt trailing edge noise can be prevented by proper design of the blades, i.e., a sufficiently small thickness of the trailing edge.

In summary, the most relevant potential noise sources for a modern wind turbine are trailing edge noise, inflow turbulence noise and tip noise. In the next section the characteristics of the different airfoil noise sources will be discussed in more detail.

4 Characteristics of airfoil noise

In this section we will first address some general theoretical aspects of the interaction between turbulence and an airfoil surface. Next, we will focus on the theoretical and experimental characteristics of trailing edge noise and other airfoil noise sources. Finally, we will consider the effect of source motion on the frequency and level of the radiated sound.

4.1 Interaction between turbulence and an airfoil surface

For the flow around the outer part of a wind turbine blade, the Mach number $M = U/c$, with c the speed of sound (about 340 m/s), is of the order of 0.2. At these low Mach numbers, *free* turbulence (away from the blade surface) is a very inefficient noise source. Therefore, the radiated aerodynamic sound from an airfoil will be dominated by the *interaction* between the turbulence and the airfoil surface. The acoustic effect of the turbulent flow depends on the length scale Λ of the turbulent eddies [10]. For trailing edge noise this turbulent length scale is the boundary layer displacement thickness δ^* at the trailing edge, for inflow turbulence noise it is the scale of the incident eddies. For a mean flow velocity U , the disturbances occur at a frequency $f \sim U/\Lambda$, which is equal to the frequency of the emitted sound $f = c/\lambda$, with λ the acoustic wavelength. Thus, if the incident eddies are much larger than the airfoil chord C , the acoustic wavelength will also be much larger than the chord, so that the airfoil is acoustically *compact*. The eddies will then cause a fluctuating force on the complete airfoil, resulting in low-frequency sound which radiates as a *compact dipole*. It can be shown analytically that in this case the acoustic power, which is proportional to the square of the acoustic pressure p , scales with the sixth power of the flow speed: $p^2 \sim U^6$. Furthermore, the radiation pattern or *directivity* is given by $p^2 \sim \sin^2 \theta$, where θ is the angle with respect to the flow direction. This directivity pattern implies that maximum radiation occurs in the direction perpendicular to the mean flow (Figure 5).

If the eddies are much *smaller* than the airfoil chord, they will induce only local pressure fluctuations which do not affect the global aerodynamic force. The sound of the turbulent eddies is scattered at the leading edge (for inflow turbulence noise) or at the trailing edge (for trailing edge noise), resulting in high-frequency *edge noise*. Using a semi-infinite flat plate approximation, it can be shown analytically that in this case the acoustic power scales with the *fifth* power of the flow speed: $p^2 \sim U^5$. Moreover, the directivity is now given by $p^2 \sim \sin^2(\theta/2)$, which means that maximum radiation occurs in the upstream direction for trailing edge noise (i.e., in the direction of the leading edge), and in the downstream direction for leading edge noise (Figure 5).

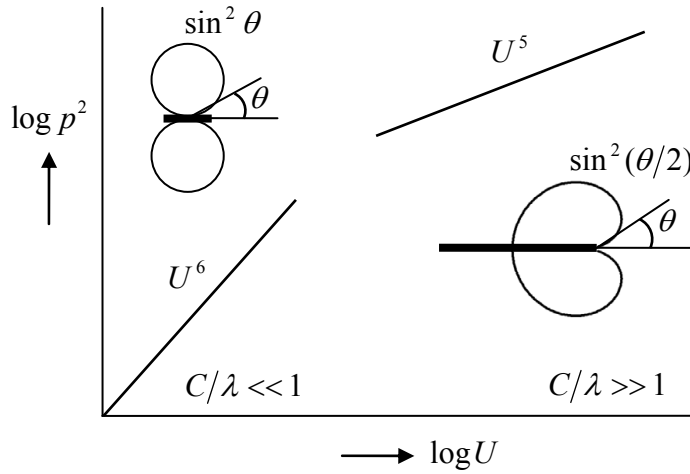


Figure 5 Directivity and speed dependence of airfoil noise [10]

Note that in Figure 5 the quantity on the x -axis is U . This is because the compactness factor $C/\lambda \sim MC/\Lambda$. Thus, for a given chord length C and turbulent length scale Λ , with increasing flow speed the source behaviour changes from a compact dipole to an edge noise source. Since for trailing edge noise the turbulence length scale is usually much smaller than the airfoil chord ($\delta^*/C \ll 1$, see previous section), the transition between the two acoustic regimes will occur at relatively low subsonic speeds. Therefore, we expect trailing edge noise to exhibit non-compact behaviour. Later in this chapter we will indeed see that the non-compact trailing edge noise characteristics match the experimental results best, even at low frequencies, where the acoustic wavelength is of the same order as the blade chord. Moreover, it will be shown that the $\sin^2(\theta/2)$ directivity largely explains the swishing character of wind turbine noise.

4.2 Theoretical relations for trailing edge noise

The trailing edge noise from a wind turbine blade is composed of the contributions from all radial segments of the blade. The characteristics of the noise from a given segment depend on the local flow parameters (Figure 6). As mentioned above, the *frequency* of trailing edge noise is proportional to U/δ^* , and is characterized by the Strouhal number $St = f\delta^*/U$: the peak of the broadband spectrum occurs at a Strouhal number of order 0.1. The *level* of the (non-compact) trailing edge noise from each radial segment can be estimated using the following expression, which was analytically derived using the semi-infinite flat plate approximation [11]:

$$p^2 \sim U^5 \frac{L\delta^*}{r^2} \cos^3 \gamma \sin^2(\theta/2) \sin \varphi. \quad (1)$$

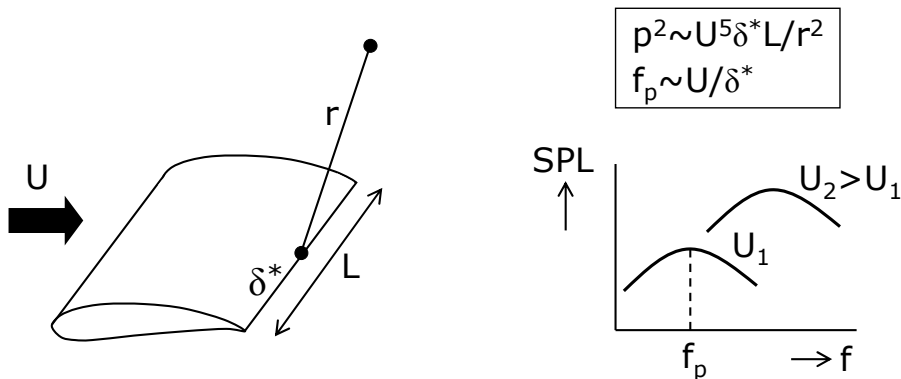


Figure 6 Trailing edge noise from a blade segment. SPL is Sound Pressure Level

In this equation, L is the span of the blade section, r is the distance between the source and the observer ($r \gg L$), and the angles are defined in Figure 7. The boundary layer displacement thickness at the trailing edge, δ^* , represents a characteristic turbulence length scale. The dependence of p^2 on L/r^2 is straightforward: doubling the span results in a doubling of acoustic energy (+3 dB), whereas a doubling of the distance results in a 75% reduction in acoustic energy (-6 dB).

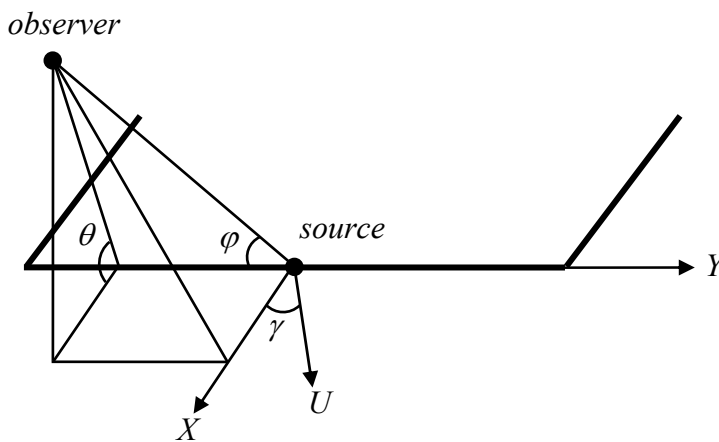


Figure 7 Definition of angles for trailing edge noise from a semi-infinite flat plate

Eq. (1) illustrates a number of interesting properties of trailing edge noise. First, we recognize the U^5 speed dependence of non-compact edge noise, as discussed in the previous section. Thus, as illustrated in Figure 6, an increase in flow speed will typically result in an increase in the level (and frequency) of the trailing edge noise spectrum (since δ^* depends only weakly on U , see previous section). This strong speed dependence of the sound level is the main reason why practically all turbine noise is produced by the outer part of the blades: doubling the flow speed (all else being equal) results in an increase in source strength of 15 dB!

The $\sin^2(\theta/2)$ directivity was also discussed in the previous section: the sound radiation is symmetrical about the chord line and maximum radiation occurs in the direction of the leading edge, where $\theta = \pi$ (Figure 8). It should be noted that, even though the pressure and suction side boundary layers contribute independently to the total noise level, the sound radiation is symmetrical. Due to scattering at the trailing edge the sound generated by the pressure side boundary layer will be radiated symmetrically (in anti-phase) to *both* sides, and the same is true for the suction side boundary layer. Since the suction side boundary layer thickness at the trailing edge, δ_s^* , is normally larger than δ_p^* , the sound produced by the suction side boundary layer usually has a higher level and lower frequency than the noise generated on the pressure side (Figure 8). The factor $\sin \phi$ in Eq. (1) describes the directivity in the lateral direction, and shows that the sound radiation goes to zero in the direction of the trailing edge.

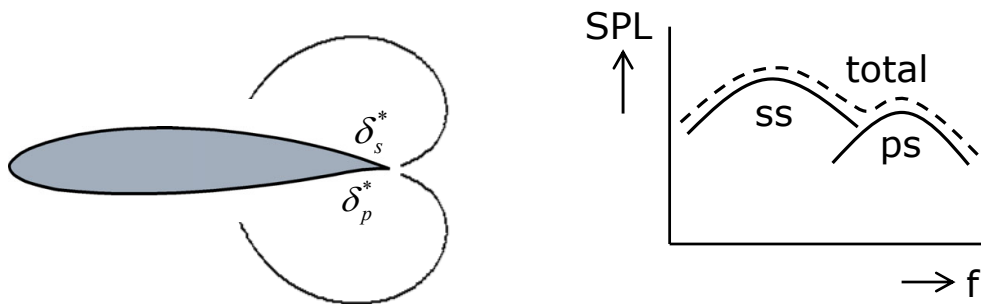


Figure 8 Directivity of trailing edge noise (left) and contributions of airfoil suction side (ss) and pressure side (ps) to total trailing edge noise spectrum (right)

The factor $\cos^3 \gamma$, finally, shows that the trailing edge scatters sound most effectively when the path of the turbulent eddies is perpendicular to the trailing edge. Thus, the sound may be reduced by sweeping the edge with respect to the flow direction (like a swept aircraft wing or a swept propeller blade). Theoretically, a sweep angle of 45° already gives a noise reduction of almost 5 dB! This idea can be extended to the use of trailing edge *serrations* (Figure 9). For a serrated trailing edge the angle between the eddy path and the edge is smaller than 90° , so that the sound is scattered less effectively [12]. This noise reduction concept will be discussed later in this chapter.

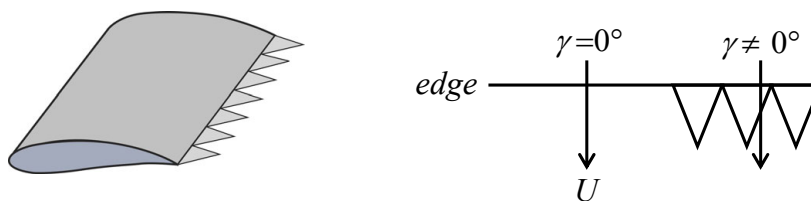


Figure 9 Trailing edge serrations

The relations described above are based on the interaction between turbulence and the trailing edge of a semi-infinite plane. As an alternative theoretical approach, trailing edge noise can also be analyzed in terms of convecting surface pressure patterns or 'gusts' [13]. This fluctuating pressure field can be regarded as the 'footprint' of the boundary layer turbulence, and its temporal and spatial transform - the wave number-frequency spectrum - can be used to compute trailing edge noise [14]. In the limits for the compact dipole and for non-compact edge noise, this theory yields the same directivity patterns as shown in Figure 5. In the transition region between these limits, where the airfoil chord is of the order of the acoustic wavelength, the directivity pattern is found to exhibit multiple lobes and a reduced intensity in the direction of the leading edge. This modified directivity pattern should be taken into account when predicting the noise from a wind turbine blade. The different trailing edge noise theories were reviewed and unified by Howe [15].

4.3 Measurements of trailing edge noise from two-dimensional airfoils

In order to verify the theoretical relations described above, in the last decades various groups have performed aeroacoustic wind tunnel tests on two-dimensional blade sections (Figure 10). Typically, these measurements are carried out in open jet wind tunnels (Figure 11). The airfoil model is mounted between two (acoustically lined) endplates and the test section is surrounded by an anechoic chamber to prevent acoustic reflections. The microphones are placed outside the tunnel flow to prevent flow-induced noise from the microphones. In some cases a phased microphone array is used to localize the noise sources on the airfoil (see Appendix 1). Several parameters may be varied, such as the wind tunnel speed, the airfoil angle of attack, and the shape of the airfoil. Furthermore, a spanwise roughness strip or *trip* may be applied to the airfoil surface, to enforce boundary layer transition from laminar to turbulent. In this way higher Reynolds numbers (where this transition occurs naturally) can be simulated. Trips may also be used to investigate the effect of surface roughness on the airfoil noise. On a wind turbine blade roughness may occur due to, for example, dirt or insects.

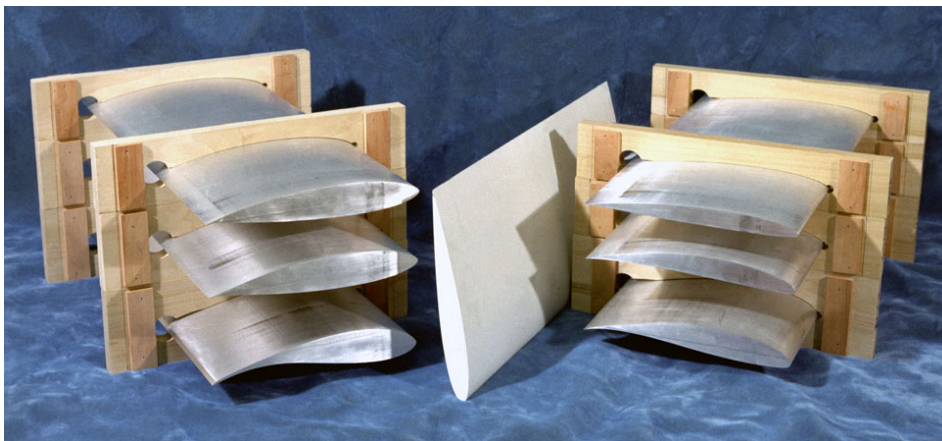


Figure 10 Two-dimensional airfoil sections for wind tunnel measurements



Figure 11 NLR's small anechoic wind tunnel KAT with white airfoil model between endplates and out-of-flow microphone array

A typical example [16] of an acoustic source map produced using a microphone array is shown in Figure 12. This map shows the noise sources on an airfoil in a clean tunnel flow (i.e., no inflow turbulence). Clearly, all noise is radiated from the trailing edge of the model. Using these maps airfoil noise spectra can be determined for different conditions. As an example, Figure 13 shows the trailing edge noise spectra for a NACA0012 airfoil at 4° effective angle of attack. Note that in open jet wind tunnels the *effective* angle of attack is usually smaller than the *geometrical* angle. This is due to the fact that the tunnel flow is deflected by the airfoil, resulting in a smaller lift force than in an infinite flow. The model chord is 0.23 m (9 inch), yielding Reynolds numbers between 0.5 and 1.1 million. It can be seen that for the clean airfoil clear spectral peaks occur, the frequency of which increases with wind speed. These spectra are indicative of laminar-boundary-layer-vortex-shedding-noise. After application of 0.25 mm trips at 5% chord on both sides of the airfoil, broadband trailing edge noise is generated, resulting in a dramatic decrease in sound levels.

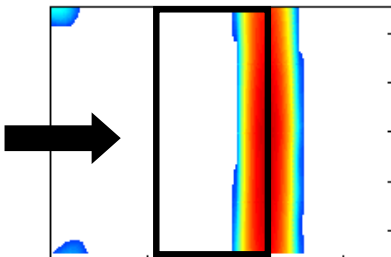


Figure 12 Acoustic source map showing trailing edge noise radiation from an airfoil in a clean flow. The black rectangle indicates the airfoil contour. Flow is from left to right

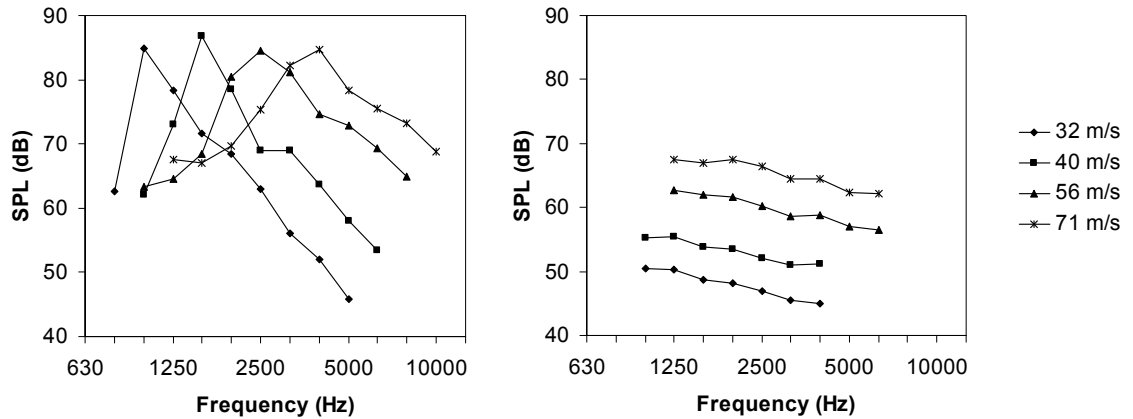


Figure 13 Airfoil noise spectra for clean (left) and tripped (right) NACA0012 airfoil at $\alpha_{eff}=4^\circ$

If we plot these trailing edge noise spectra in a normalized manner, with $SPL_{norm} = SPL - 10 \log(\delta^* U^5)$ as a function of the Strouhal number, we see that all spectra collapse on a single 'universal' curve (Figure 14). For this figure the boundary layer thickness was not measured, but roughly estimated using $\delta^*/C \approx 0.05 Re^{-1/5}$. However, similar results were also obtained using *measured* values of the displacement thickness, in a comprehensive experimental study on NACA0012 airfoils with varying chord lengths [6]. Acoustic results for other airfoil shapes and flat plates show a similar behaviour [17]. It should be noted that in some studies slightly different scaling approaches are used to obtain the best collapse of the experimental data. Nevertheless, the global dependence of the trailing edge noise spectrum on flow speed appears to be well described by the relations given in the previous section.

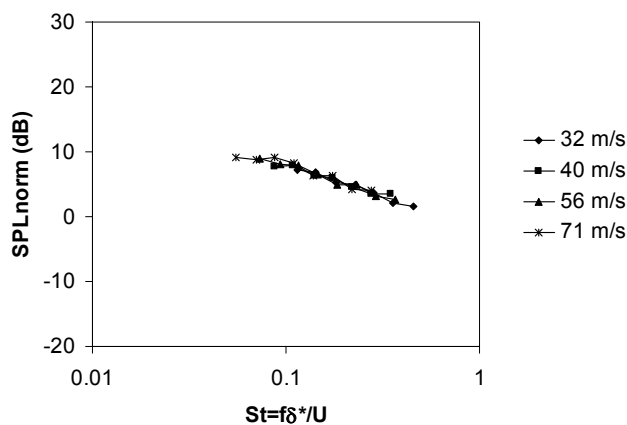


Figure 14 Normalized trailing edge noise spectra as a function of Strouhal number for tripped NACA0012 airfoil at $\alpha_{eff}=4^\circ$

The *directivity* of trailing edge noise from two-dimensional airfoils has also been investigated in wind tunnel measurements. In general, the experimental results are in accordance with the flat

plate directivity function from Eq. (1). For example, Figure 15 shows that the sound radiation is symmetrical with respect to the chord line, even though the flow is asymmetrical due to the nonzero angle of attack. However, due to geometrical constraints in the wind tunnel, experimental validation of the directivity function has been limited to the plane normal to the trailing edge, for directions not too close to the plane of the airfoil [18]. Thus, the directivity function has only been validated for $\phi=90^\circ$ and approximately $45^\circ < |\theta| < 135^\circ$. We will see later that the characteristics of wind turbine noise can be used to assess the complete trailing edge noise directivity function.

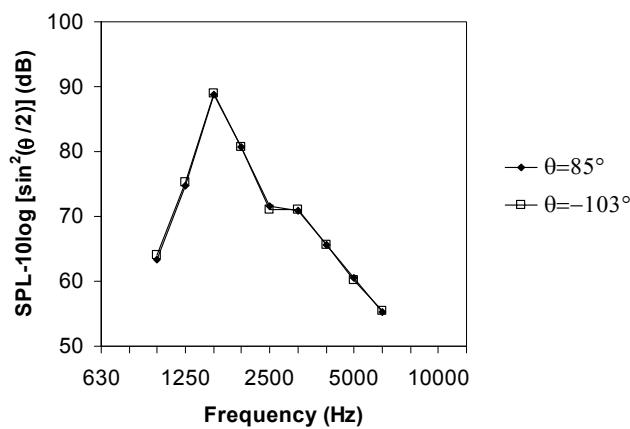


Figure 15 Airfoil noise spectra for clean NACA0012 airfoil at 40 m/s and $\alpha=4^\circ$.

4.4 Blunt trailing edge noise

Blunt trailing edge noise occurs when the trailing edge thickness h is increased above a critical value. If the ratio h/δ^* is larger than about 0.3, periodic vortex shedding may occur, resulting in a Von Karman type vortex street. The alternating vortices in the near wake produce surface pressure fluctuations close to the trailing edge, leading to tonal noise. The frequency of the tone is determined by the Strouhal number $St = fh/U \sim 0.1$. Thus, sharpening of the trailing edge will shift the peak towards the ultrasound region. As h increases, the frequency and the bandwidth of the tone decrease, but the broadband part of the spectrum remains the same as for a sharp edge. Since for a wind turbine blade the flow speed varies along the radius, blunt trailing edge noise may not result in a single tone or hump in the spectrum, but may rather appear as a broadband spectral increase.

The directivity and speed dependence of blunt trailing edge noise are considered to be the same as for broadband trailing edge noise: for $C/\lambda < 1$ the source behaves like a compact dipole with $\sin^2 \theta$ directivity and U^6 speed dependence, while for $C/\lambda > 1$ it is an edge noise source with $\sin^2(\theta/2)$ directivity and U^5 speed dependence. The amplitude of blunt trailing edge noise also depends strongly on the trailing edge geometry (Figure 16). A round shape or a

60°-90° wedge may produce amplitudes two or three times higher than a rectangular edge, while a wedge angle smaller than 45° or a bevel angle less than 60° can give much lower amplitudes [10].

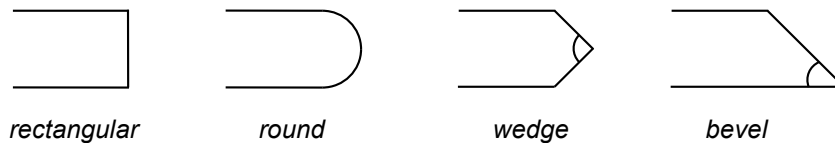


Figure 16 Blunt trailing edge geometries

4.5 Inflow turbulence noise

The characteristics of inflow turbulence noise depend strongly on the properties of the incoming turbulence. As mentioned above, turbulent eddies with a length scale Λ much larger than the airfoil chord will lead to compact dipole noise with a $\sin^2 \theta$ directivity and a U^6 speed dependence. Small eddies will induce local pressure fluctuations, causing leading edge noise with a U^5 speed dependence. On the basis of the semi-infinite flat plate approximation, a $\sin^2((\pi - \theta)/2)$ directivity pattern is expected, with maximum radiation in the direction of the trailing edge (i.e., the pattern is inverted with respect to trailing edge noise). However, the actual directivity pattern will depend on the details of the airfoil geometry. The frequency of the radiated sound is given by $f \sim U/\Lambda$. Thus, the spectrum of inflow turbulence noise is directly related to the spectrum of the incoming turbulence. Natural atmospheric turbulence is expected to cause broadband noise for frequencies up to 1000 Hz. Other sources of inflow turbulence may be the tower wake (for downwind rotors) or the turbulent wake from upwind turbines in a wind farm. It is currently still an open issue to what extent inflow turbulence noise contributes to the overall sound level of a large wind turbine [19]. For small wind turbines inflow turbulence noise may be more important, because these are often placed in a turbulent environment (e.g. rooftops). Moreover, small-scale turbulence produces higher frequencies, which are closer to the center of the audible range, while for small turbines the dominant trailing edge noise frequencies are beyond this range.

The characteristics of inflow turbulence noise were investigated experimentally [16] in the same wind tunnel as described above for trailing edge noise (Figure 11). Inflow turbulence was generated using a turbulence grid inside the nozzle. The grid had diagonally oriented 12-mm bars and a mesh width of 60 mm. The turbulence in a flow can be quantified using the *turbulence intensity*, which is the ratio of the root-mean-square of the velocity fluctuations and the mean flow speed. The present grid produced turbulence with an intensity of about 11% at the leading edge of the airfoil (without grid the turbulence intensity was 1% or less). It should be noted that this level of turbulence is much higher than that which is usually experienced in the atmosphere at typical rotor speeds.

The source map in Figure 17 shows that in the presence of severe inflow turbulence leading edge noise is dominant. The corresponding spectra in Figure 18 illustrate the dependence on wind speed. First, we see that tripping does not affect inflow turbulence noise. This is not surprising, since the leading edge noise depends on the turbulence in the inflow, and not on the boundary layer. Interestingly, the normalized plot shows that the best data collapse is obtained if the data is scaled using the *sixth* power of the tunnel speed. Thus, in contrast to the trailing edge noise discussed above, inflow turbulence noise appears to behave like a compact dipole, at least in this experiment. Similar to the trailing edge noise, the inflow turbulence noise radiation was found to be symmetrical with respect to the chord line.

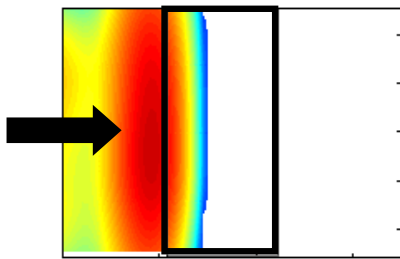


Figure 17 Acoustic source map showing leading edge noise radiation from an airfoil in a turbulent flow. The black rectangle indicates the airfoil contour. Flow is from left to right

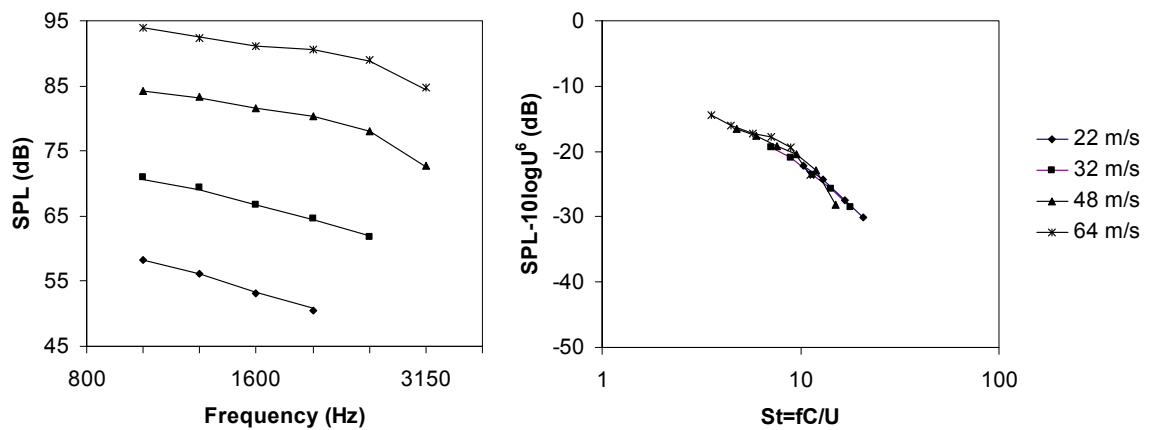


Figure 18 Inflow turbulence noise spectra for S822 airfoil at $\alpha_{eff}=8^\circ$. Left: measured spectra with trip (markers) and without trip (lines). Right: normalized spectra

The dependence of inflow turbulence noise on airfoil shape was also investigated. Figure 19 shows the leading edge noise spectra together with the airfoil shapes, in order of decreasing sound level. It can be clearly seen that the inflow turbulence noise level increases with increasing 'sharpness' of the leading edge (or decreasing airfoil thickness). This trend is well reproduced by semi-empirical prediction codes [20].

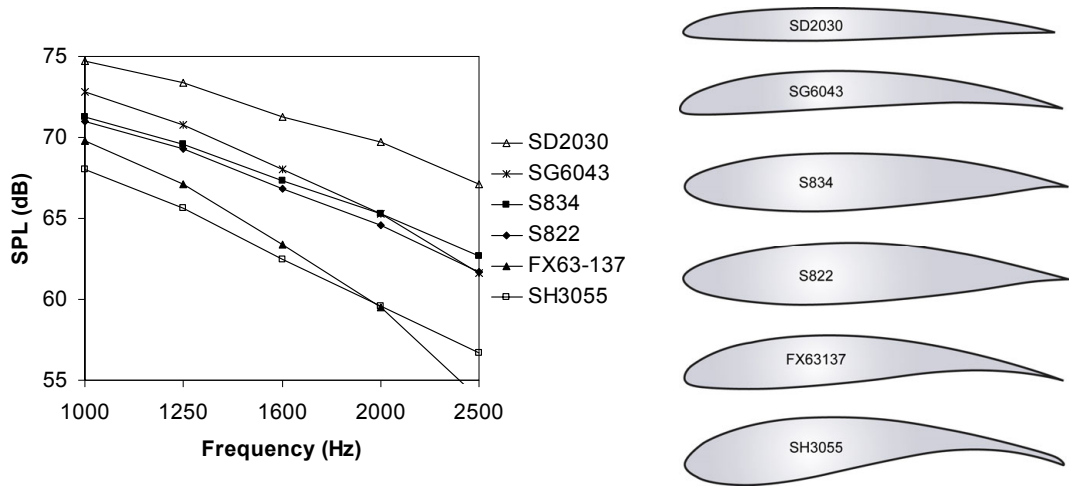


Figure 19 Inflow turbulence noise spectra for different airfoils at 32 m/s and $\alpha_{eff}=8^\circ$. The airfoil shapes are plotted in order of decreasing sound level

4.6 Tip noise

Tip noise is caused by the three-dimensional flow at the very tip of the blade. Due to the pressure difference between the pressure and suction side of the blade, a tip vortex is formed. Turbulence is convected over the tip edge and separated flow may occur. The mechanism of noise production can be considered to be the same as for trailing edge noise [6]. Thus, we expect the frequency and level of tip noise to depend on the (spanwise) length scale of the tip vortex and the convection velocity over the edge. These parameters are again related to the blade load distribution, the strength of the tip vortex, and the planform shape of the tip [4]. Tip noise typically has a broadband, high frequency character and is not considered to be the most important noise source for modern large wind turbines. Nevertheless, it can make a significant contribution to the total sound level in specific cases. Blade tip noise is related to flap side-edge noise from aircraft wings, although a flap tip usually has a rectangular planform and a flat side-edge. Noise reduction concepts for flap edge noise include fences [21] (similar to winglets) and porous edges [22].

4.7 Moving sources

For rotating wind turbine blades the sound source is moving with respect to the (stationary) observer. In this section we will discuss the effect of source motion on the frequency and level of the perceived sound. Consider a sound source moving at speed U in a stationary medium and radiating sound at frequency f . The frequency perceived by a stationary observer is then given by

$$f' = \frac{f}{1 - M \cos \vartheta}, \quad (2)$$

with $M = U/c$ and \mathcal{G} the angle between the source velocity and the source-observer line (at emission time). This is the well-known *Doppler frequency shift*. If the source moves towards the observer the perceived frequency increases, and vice versa. For sound from a rotating wind turbine blade with a tip Mach number of 0.2, a Doppler factor of 1.25 is found for an observer in the rotor plane. This means that during the blade revolution the perceived frequency of a 1 kHz signal varies between 830 Hz and 1250 Hz!

Besides the frequency shift, source motion also affects the *amplitude* of the perceived sound. This effect is called Doppler or convective amplification, and its magnitude depends on the nature of the source. For the low Mach number aerodynamic noise sources on wind turbine blades, the amplitude p of the perceived sound is modified by the factor

$$\frac{1}{(1 - M \cos \mathcal{G})^2} \quad (3)$$

This means that the sound level increases when the source moves towards the observer and vice versa. For a wind turbine blade rotating at a tip Mach number of 0.2, this factor amounts to 3-4 dB for an observer in the rotor plane. So even if the source has a constant strength and a uniform directivity, the observer in the rotor plane will perceive a variation in sound level of 7 dB during the revolution of the blade! This example illustrates that we have to account for convective effects in the analysis or prediction of wind turbine noise.

It should be noted that, while the frequency shift is determined by the velocity of the source relative to the *observer*, the amplification factor depends on the speed with respect to the *medium*. Thus, in the acoustic wind tunnel tests described above, we have to account for convective amplification, although there is no frequency shift.

5 Field measurements of wind turbine noise

This section deals with acoustic field measurements of wind turbine noise [23,24]. First, we will discuss some features of wind turbine noise that can be measured with a single microphone. Next, source localization measurements with a phased microphone array are considered. These experiments will be used to explain the swishing character of the noise and to show that trailing edge noise from the blades is the dominant source mechanism.

5.1 Single-microphone measurements

Several interesting features of wind turbine noise can be measured with a single microphone. Figure 20 shows a picture of the turbine that will be used throughout this chapter to illustrate the different aspects of the sound. The three-bladed rotor has a diameter of 94 m and the tower

height is 100 m. The three blades are not cleaned, tripped or treated otherwise. The turbine is pitch-controlled and has a rated power of 2.3 MW.



Figure 20 A typical modern large wind turbine. The noise source distribution in the rotor plane (averaged over many revolutions) is projected on the picture

The average spectrum of this turbine is shown in Figure 21. It can be seen that the turbine produces broadband noise, with the highest levels between 315 Hz and 1250 Hz. The absence of spectral peaks or humps suggests that mechanical noise is not important for this turbine, and that blade noise is dominant. By integrating this spectrum we can calculate the overall sound pressure level OASPL of the turbine, and investigate how it depends on wind speed (Figure 22). Note that rather than wind speed, in this figure the sound levels are plotted as a function of power, because this quantity was measured more accurately. It can be seen that the noise increases only gradually with increasing wind speed. This can be intuitively understood from the fact that the effective flow speed perceived by the blades increases only slowly with wind speed. It should be noted that wind turbine noise is most annoying at low wind speeds, when background noise levels are low. This is reflected in the IEC norm for wind turbine noise measurements [25], which demands measurements between wind speeds of 6 m/s and 10 m/s (at 10 m height).

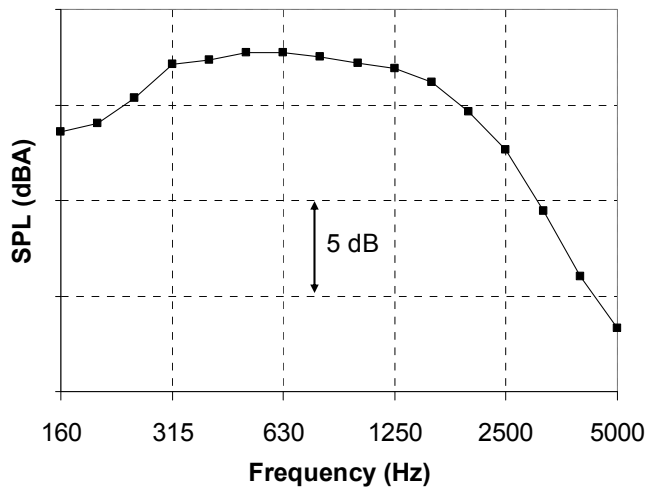


Figure 21 Wind turbine noise spectrum

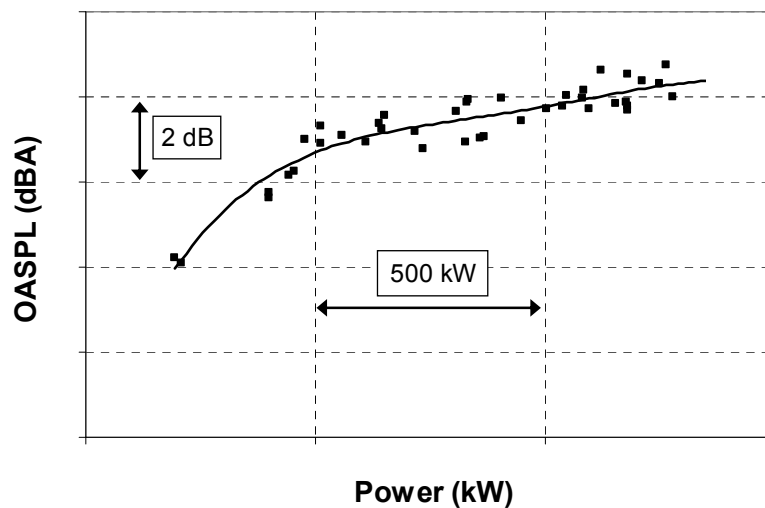


Figure 22 Wind speed dependence of turbine noise (measured values and trend line)

The measurements discussed above were taken with a microphone on a ground plate, about one rotor diameter upwind of the turbine. By carrying out measurements at different locations, the *directivity* of the wind turbine noise can be determined. This will be discussed in more detail later, in relation to the prediction of wind turbine noise.

Rather than considering *averaged* sound levels, we can also look at the sound level as a function of time (Figure 23). In order to show the dependence on blade position more clearly, the sound level variation is shown as a function of rotor azimuth. For both measurement locations we can clearly identify three humps, corresponding to the passage of the blades. This amplitude modulation of the broadband aerodynamic blade noise at the blade passing frequency is often referred to as *swish*. It can be seen that for an observer close to the rotor plane the swish

is much more pronounced than at an upwind position. Furthermore, the level variations for these two positions are in anti-phase. As expected, the noise levels from the three different blades are practically the same.

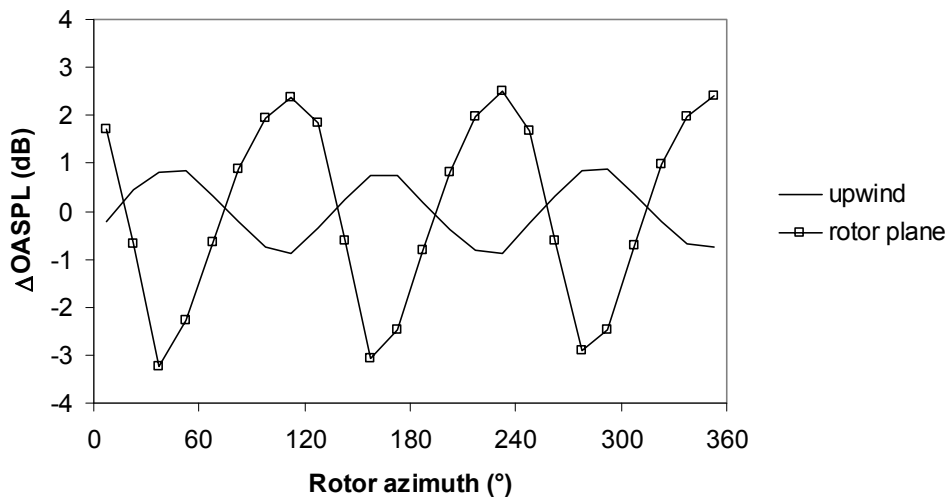


Figure 23 Sound level variation as a function of rotor azimuth, for two measurement locations at about one rotor diameter distance from the turbine

The above results illustrate that single-microphone measurements are useful for quantifying and characterizing the noise from wind turbines. However, in order to understand the measured trends, and to be able to predict and reduce wind turbine noise, we would like to know what the dominant *source* is. It may be trailing edge noise, but also for instance inflow turbulence noise or tip noise. In order to get more information about the source mechanisms we have to revert to source localization techniques. This is the subject of the next section.

5.2 Noise source distribution in the rotor plane

Source localization measurements were done using a 148-microphone acoustic array, mounted on a horizontal wooden platform of about 16x18 m² (Figure 20 and Figure 24). The distance between the platform and the tower was roughly the same as the tower height, resulting in a 'view angle' of about 45°. By placing the scan plane of the array in the rotor plane, the noise source distribution in the rotor plane could be determined (Figure 25). It is important to realize that no assumptions or adjustable settings were used to produce these results. The source maps simply show from what direction the sound is coming, for an observer at the platform position. Also note that the source distribution is averaged over a large number of revolutions (more than 20 minutes of measurement time), covering the wind speed range between about 6 m/s and 10 m/s.

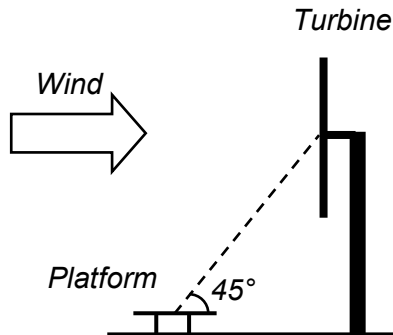


Figure 24 Test set-up for array measurements on a wind turbine

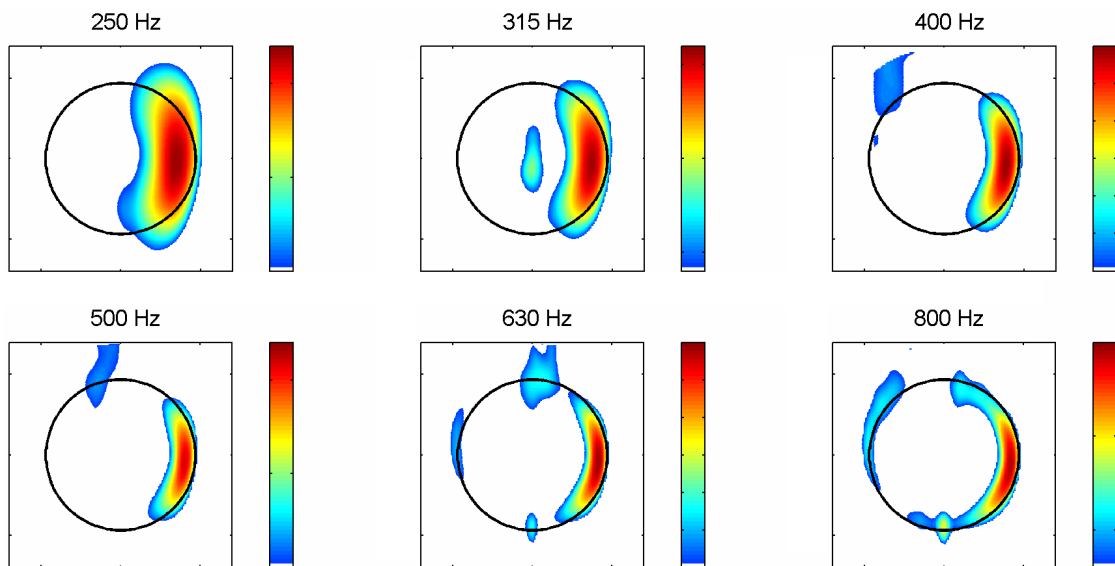


Figure 25 Average noise source distribution in the rotor plane as a function of frequency. The turbine rotates in clockwise direction and the tip trajectory is indicated by the black circle. The range of the colour scale is 12 dB

Several interesting observations can be made in Figure 25. First, we see that practically all noise is produced by the blades, although the nacelle also generates some noise at 315 Hz. Note that the 'sources' between 10 and 12 o'clock for 400 Hz - 630 Hz are an artefact of the array technique. Second, most of the noise is radiated from the outer part of the blades, but not the very tip. This rules out tip noise as the dominant noise source. The dominance of the outer part of the blades can be understood from the fact that aerodynamic noise scales with the 5th or 6th power of the flow speed, as discussed before. We can also observe a minor high-frequency source where the blades pass the tower. This may originate from (1) reflection of blade noise on the tower, (2) impingement of blade tip vortices on the tower, and/or (3) the upstream influence of the tower on the flow field around the blade. However, the most striking feature in the source maps is that practically all noise is produced during the downward movement of the blades.

This asymmetric source pattern explains the swishing character of the noise perceived on the ground (Figure 23): each time a blade passes the 3 o'clock position, a swish is radiated to the observer at the array position. Note that by the time the sound arrives at the observer, the blade has already travelled further. As a result, the swish sometimes *seems* to be generated when the blade is close to the tower.

Now the remaining question is *why* the source distribution in the rotor plane is asymmetric. Assuming that the effects of wind shear and rotor tilt angle are small, the flow conditions on the blade, and consequently the acoustic source strength, are independent of rotor azimuth. In other words, the blades produce a constant sound level during the complete revolution. Therefore, we expect the strong asymmetry to be due to convective and directivity effects. The trailing edge noise directivity function in Eq. (1) exhibits maximum radiation in the direction of the leading edge. Thus, if the blade moves downward, the trailing edge noise is mainly radiated towards the ground, while if the blade moves upward the noise radiates into the sky. As a result, an observer on the ground will hear the trailing edge noise mainly when the blades move downward. Furthermore, the convective factor in Eq. (3) shows that the amplitude of the perceived sound increases when the source moves towards the observer, and decreases when it moves away from the observer. Again, this means that the descending blade will be noisier than the ascending blade for an observer on the ground. Thus, the characteristics of trailing edge noise seem to be qualitatively in line with the experimental results.

To see if trailing edge noise directivity and convective amplification can *quantitatively* explain the observed asymmetry, the magnitude of both effects, given by the factor

$$\frac{\sin^2(\theta/2)\sin\phi}{(1-M\cos\vartheta)^4} \quad (4)$$

is calculated for an observer on the ground, one rotor diameter upwind from the turbine. The source is assumed to be located at the tip of the blade, which rotates at a Mach number of 0.2. For simplicity the rotor tilt angle and the blade pitch and twist are assumed to be zero. Figure 26 shows the magnitude of the directivity and convective factors in Eq. (4) as a function of rotor azimuth (0° corresponds to the 12 o'clock position). As expected both effects increase the perceived sound level during the downward movement of the blades, and decrease the level during the upward movement. The directivity factor has the largest effect. The total asymmetry is more than 12 dB and the maximum occurs between 3 and 4 o'clock, which is in good agreement with the acoustic source maps in Figure 25. Thus, the asymmetry in the source maps can be well explained using the characteristics of trailing edge noise.

Now the question is what the source distribution would look like if the dominant source mechanism were inflow turbulence noise or compact dipole noise. The convective amplification

factor for these sources is the same as for trailing edge noise, but as discussed before the directivity factor is different: for inflow turbulence (leading edge) noise, maximum radiation occurs in the direction of the trailing edge, while a compact dipole radiates strongest in the direction perpendicular to the plane of the blade. The magnitude of these directivity factors (including convective amplification) is shown in Figure 27, again for an observer on the ground, one rotor diameter upwind from the turbine. As a reference the curve for non-compact trailing edge noise is shown as well.

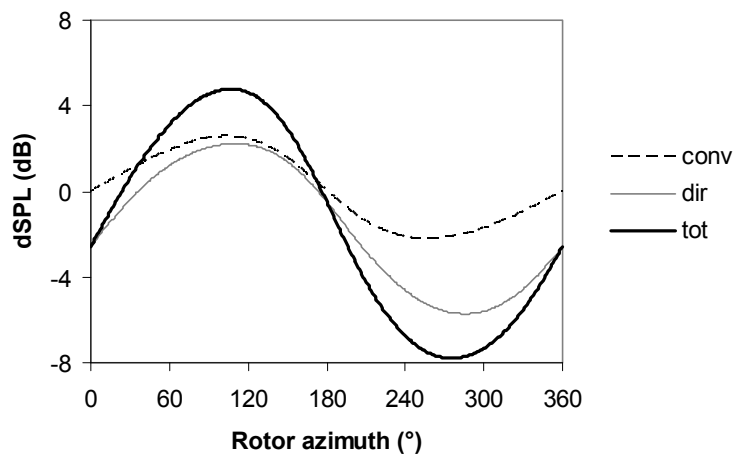


Figure 26 Calculated convective amplification and directivity factors for non-compact trailing edge noise

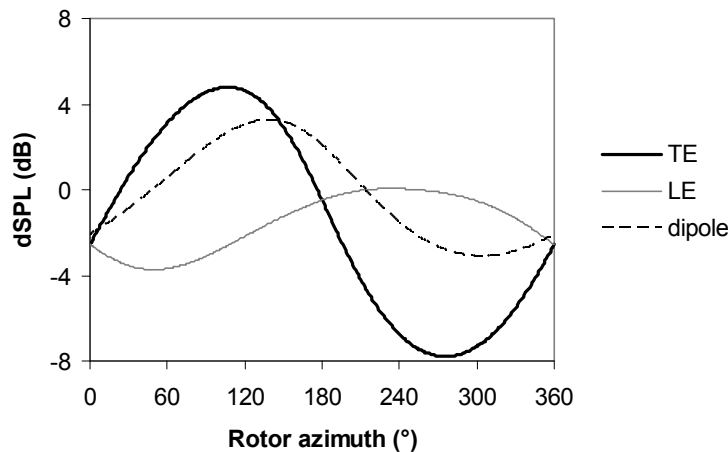


Figure 27 Calculated effect of convective amplification and directivity for non-compact trailing edge noise, non-compact leading edge noise, and compact dipole noise

It can be seen that for leading edge noise the maximum level would be radiated during the *upward* movement of the blades, while for a compact dipole the asymmetry would be less than 8 dB. Thus, the experimental results can *only* be explained using the directivity function for non-compact trailing edge noise. This is true even at the low frequencies, where the acoustic

wavelength is of the same order as the blade chord. Thus, the blades produce a constant sound level during the complete revolution, but the trailing edge noise radiates mainly in the direction in which the blade is moving. As a result, an observer on the ground hears the blades most clearly during their downward movement, which causes the swishing character of the sound. It should be noted that the asymmetry in the source maps is purely an effect of observer position: an observer above the turbine would mainly hear the ascending blades, while an observer on the rotor axis would perceive a circular source pattern, without swish. We will further discuss the swish amplitude for different observer locations, as shown in Figure 23, in the section about the prediction of wind turbine noise.

We can also use the trailing edge noise characteristics to explain the fact that in Figure 25 the source radius increases with increasing frequency. As mentioned before, the peak frequency of trailing edge noise is proportional to U/δ^* . For increasing radius the flow speed increases, and the boundary layer thickness typically decreases due to the smaller blade chord. Thus, the frequency of the emitted sound increases with increasing radius.

5.3 Noise sources on the blades

In addition to the source distribution in the rotor plane, array measurements can also be used to identify the noise sources on the individual blades. This is done by defining three rotating scan planes which move along with the blades. To investigate the effect of different blade treatments, measurements were done on an 850 kW wind turbine with one cleaned blade, one tripped blade, and one untreated blade. The rotor diameter was 58 m. Tripping was done using zigzag tape of 0.4 mm thickness over the complete radius, at 5% chord on the suction and pressure side of the blade. Like the turbine discussed above, practically all perceived noise was produced by the outer part of the blades, during the downward part of the revolution.

The source maps for the individual blades, shown in Figure 28, are in line with this. Moreover, the corresponding noise spectra show that the tripped blade is much noisier than the other two, especially at low frequencies. This can be explained by the characteristics of trailing edge noise: tripping leads to a thicker boundary layer, which in turn yields lower frequencies and higher sound levels. Since tripping was previously found to have no effect on inflow turbulence noise (Figure 18), these results are another indication that trailing edge noise is the dominant mechanism (at least after tripping). This was further confirmed by the fact that the blade noise spectra are proportional to the fifth power of the local flow speed. Moreover, analysis of the narrowband noise spectra for individual radial stations of the blade shows that tonal blunt trailing edge noise is not important for these turbines.

All in all, the experimental results for both turbines provide strong evidence that trailing edge noise is the dominant noise source for typical modern wind turbines. This fact will be used in the next section to develop a wind turbine noise prediction method based on trailing edge noise characteristics.

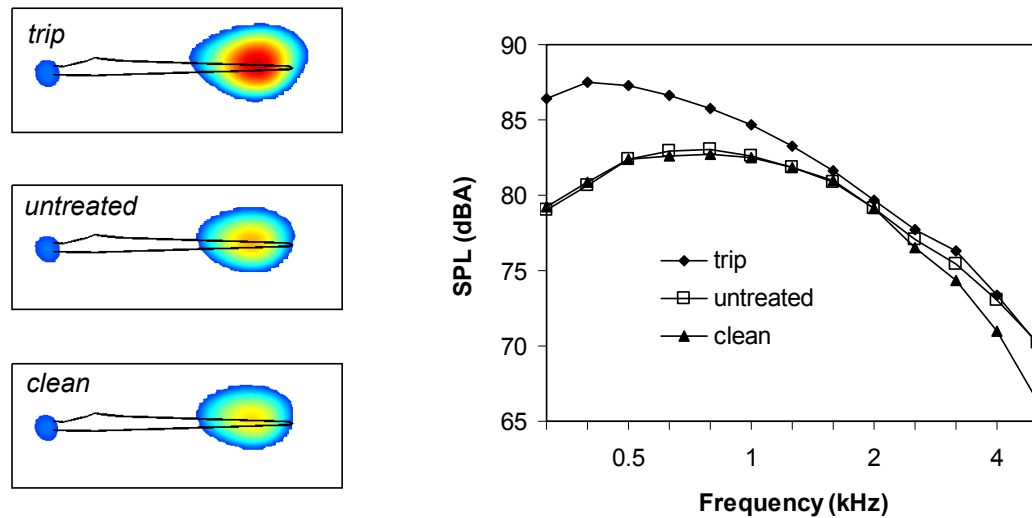


Figure 28 Acoustic source maps (800 Hz) for individual blades and corresponding noise spectra. The black line indicates the blade contour (leading edge on lower side). The range of the colour scale is 12 dB and the scale is the same for the three blades

6 Prediction of wind turbine noise

The ability to predict wind turbine noise is essential for the design of quiet turbines and for assessing possible noise pollution around wind farms. There are several different approaches to calculating the noise from a wind turbine, with different degrees of sophistication. On one side of the spectrum we have the 'rule-of-thumb' methods, which only need the rotor diameter or rated power as input. Although these empirical methods can provide an order-of-magnitude estimate of the sound level, they do not enable us to assess design modifications or noise characteristics. On the other side of the spectrum, we have complete numerical methods, which combine Computational Fluid Dynamics (CFD) and Computational AeroAcoustics (CAA) to calculate the sound of an airfoil section from first principles. These methods are computationally rather expensive and at present do not allow us to calculate the sound from a complete three-dimensional wind turbine rotor with high Reynolds number flow around the blades.

Somewhere in between these two extremes we have the semi-analytical, semi-empirical methods. These models contain scaling laws derived from theoretical analyses, and are complemented with results from aerodynamic and acoustic measurements. The different potential source mechanisms are considered separately. This type of method represents the current state-of-the art and will also be applied in the present section [26]. The models are based on physical relations and therefore allow us to investigate the influence of several design and operation parameters, such as the blade planform, blade twist, airfoil shape, pitch angle, RPM,

and wind speed. At the same time they are fast enough to allow a quick assessment of different design modifications. Moreover, we will see below that these methods are capable of producing *accurate* predictions.

In the previous section we saw that trailing edge noise is the dominant noise source for typical modern wind turbines. In the present section we will use this knowledge to develop a semi-analytical, semi-empirical prediction method for wind turbine noise. First, the prediction method is described in detail. Then, the predictions will be validated against experimental results. Finally, the prediction method will be applied to calculate the noise footprint of a typical wind turbine.

6.1 Prediction method

Since the field measurements show that broadband trailing edge noise is the dominant noise source for both turbines, only this noise source is incorporated in the prediction method. This means that inflow-turbulence noise, blunt trailing edge noise, and tip noise are discarded. The prediction method only needs the blade geometry and turbine operating conditions as input, and contains no fitting or tuning parameters. The calculation can be divided into three steps: (1) blade aerodynamics, (2) trailing edge noise source strength, and (3) directivity and convective amplification. These steps will be described in the following.

First, the blade is divided into a number of radial segments (21 for the present calculations). For each segment, the local flow parameters (Reynolds number, angle of attack) are calculated using a blade element momentum method. An airfoil design and analysis code is then used to calculate the boundary layer displacement thicknesses on the pressure and suction side. The effects of atmospheric turbulence, wind shear, and yaw are neglected in the calculations, i.e., stationary and axisymmetric conditions are assumed.

In the second step, the source spectrum for each radial segment is calculated using a semi-empirical, semi-analytical prediction code for trailing edge noise from two-dimensional airfoil sections [6]. This code is based on comprehensive acoustic and aerodynamic measurements on NACA0012 airfoils with varying chord lengths, at various flow speeds and angles of attack. The total trailing edge source strength due to the turbulent boundary layer is the sum of three contributions of the following form:

$$SPL_i = 10 \log \left(\frac{\delta_i^* M^5 L}{r^2} \right) + A_i \left(\frac{St_i}{Sr_i} \right) + K_i, \quad (5)$$

where δ^* is the displacement thickness, M the Mach number, L the span of the blade segment, r the distance to the observer, and K an empirical constant which depends on the Mach and Reynolds numbers. The function A describes the spectral shape as a function of the ratio between the Strouhal number $St = f \delta^* / U$ (with U the local flow speed) and the

empirical peak Strouhal number Sr . The three contributions (here denoted by the index i) are the pressure side boundary layer, the suction side boundary layer, and an additional contribution to account for nonzero angle of attack. Note that Eq. (5) is essentially a combination of the analytical relation in Eq. (1) (without the directivity factors), and an empirically found 'universal' normalized trailing edge noise spectrum, similar to Figure 14.

In the third step, directivity and convective effects are included to obtain the effective source strength perceived by an observer at a specified position. These effects are accounted for using a modified version of Eq. (4). The numerator in this equation describes the directivity for trailing edge noise from a semi-infinite flat plate, and has maximum radiation in the direction of the leading edge. However, as mentioned before, the directivity function for a finite-chord airfoil exhibits a reduced intensity in the direction of the leading edge. Therefore, the numerator of Eq. (4) is modified to reflect this finite-chord effect. The corresponding directivity functions are shown in Figure 29. In these plots, the source position at the trailing edge is located at the centre of the sphere, the chord line runs along the x -axis and the trailing edge runs along the y -axis. Note that this modification only affects the sound at observer positions close to the rotor plane, which means that the results in Figure 26 and Figure 27 (for an upwind observer) are still valid.

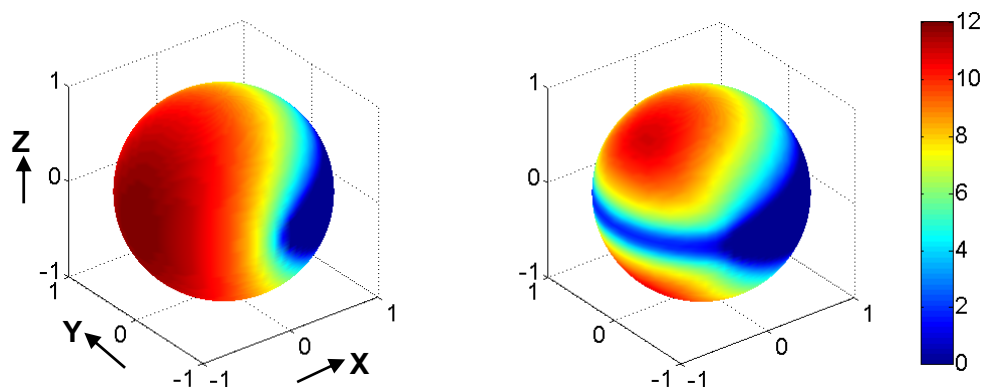


Figure 29 Trailing edge noise directivity function for semi-infinite flat plate (left) and finite-chord airfoil (right). The range of the colour scale is 12 dB

6.2 Validation against experiment

In order to validate the prediction method, calculations were carried out for both turbines mentioned in the field measurements section. In the present section we will show some representative comparisons between prediction and experiment for the 2.3 MW turbine shown in Figure 20. First, Figure 30 shows the measured and calculated overall sound level as a function of rotor power. It can be seen that the trend in the experiments is well represented by the predictions: the difference between measurement and prediction is less than 1-2 dB, which is smaller than the scatter in the experimental data. For the other turbine a similar agreement was found. This accuracy is considered satisfactory for the present semi-empirical prediction model.

Besides the overall sound level, also the *shape* of the predicted rotor noise spectrum (not shown here) was found to agree well with the experiments.

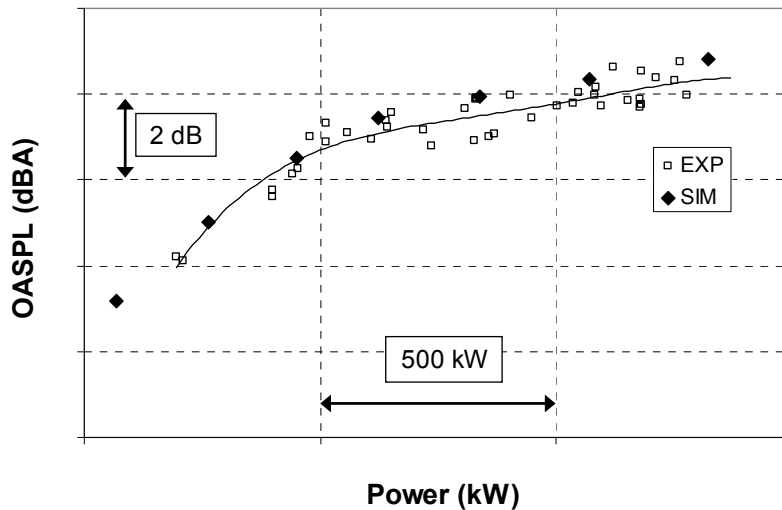


Figure 30 Measured and predicted rotor noise levels as a function of rotor power

In order to assess the directivity of the turbine noise, in the experiments eight ground microphones were placed on a 240-m circle around the turbine, at 45° intervals (Figure 31). In this figure, β indicates the misalignment angle between turbine and array, and ξ indicates the position of a ground microphone with respect to the downwind direction. The measured and calculated directivity are shown together in Figure 32. The experimental directivity pattern shows two dips in the crosswind directions, i.e., for measurement positions close to the rotor plane ($\xi = 90^\circ$ and $\xi = 270^\circ$). The predicted curve follows the measured curve within 1-2 dB, with two 6 dB dips in the cross-wind direction. These dips can be understood from the reduced levels of the trailing edge noise directivity function close to the plane of blade (Figure 29).

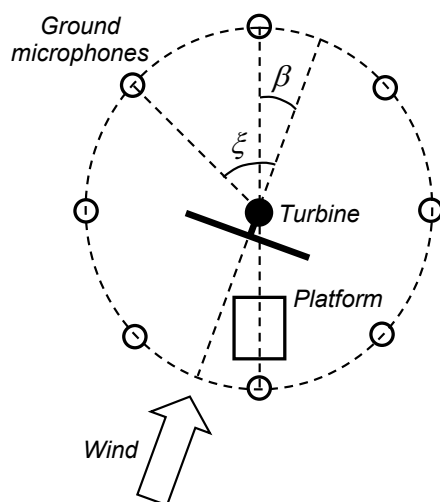


Figure 31 Top view of test set-up for directivity measurements

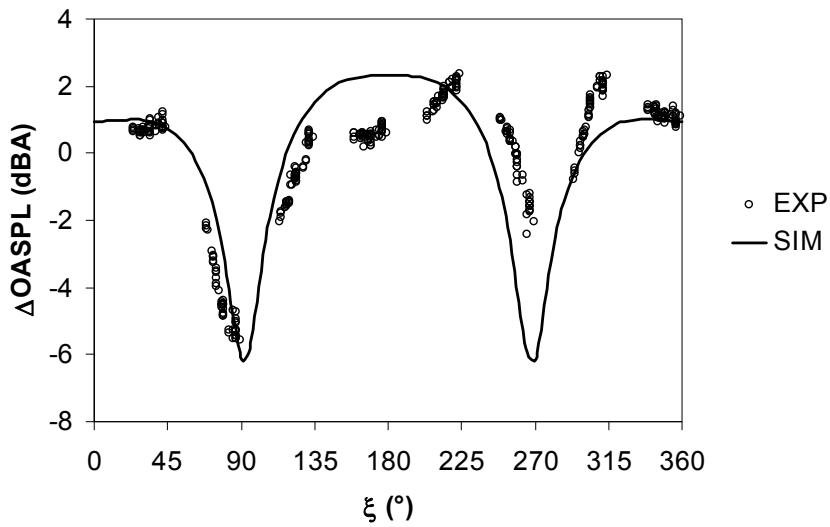


Figure 32 Measured and predicted turbine noise directivity

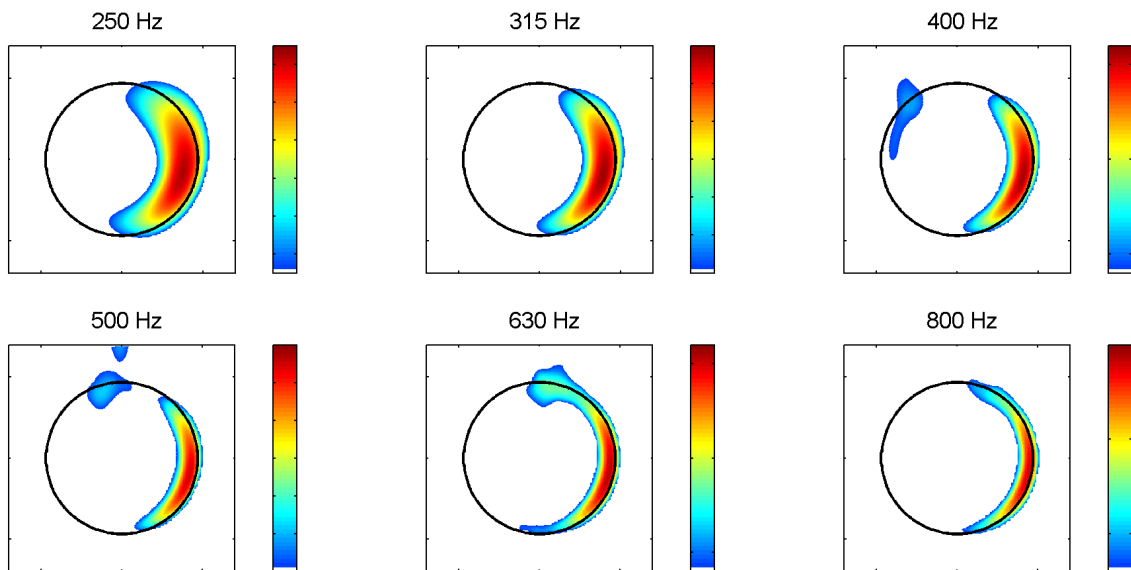


Figure 33 Predicted source maps (compare to measured maps in Figure 25)

The calculated source distribution in the rotor plane was also used to produce simulated source maps (Figure 33). Comparison with the measured source maps in Figure 25 shows good agreement: as in the experiments, the simulated source maps show dominant noise radiation from the outer part of the blades, during their downward movement. Furthermore, the blade sources move outward with increasing frequency.

Whereas the previous source maps concern misalignment angles β around 0° , experimental data are also available for large misalignment angles. The measured and predicted

source maps for these angles are shown in Figure 34. It can be seen that the location of the source region shifts upward or downward when the right or left hand side of the rotor plane is turned towards the array, respectively. This can be qualitatively explained by the change in the component of the blade velocity in the direction of the array, which results in a change in convective amplification. In short: you mainly hear the blade when it is coming towards you. At high misalignment angles the array resolution decreases due to the oblique view angle. Again a good qualitative agreement between simulation and experiment is found, indicating that the changes in source pattern are well captured by the trailing edge noise prediction method.

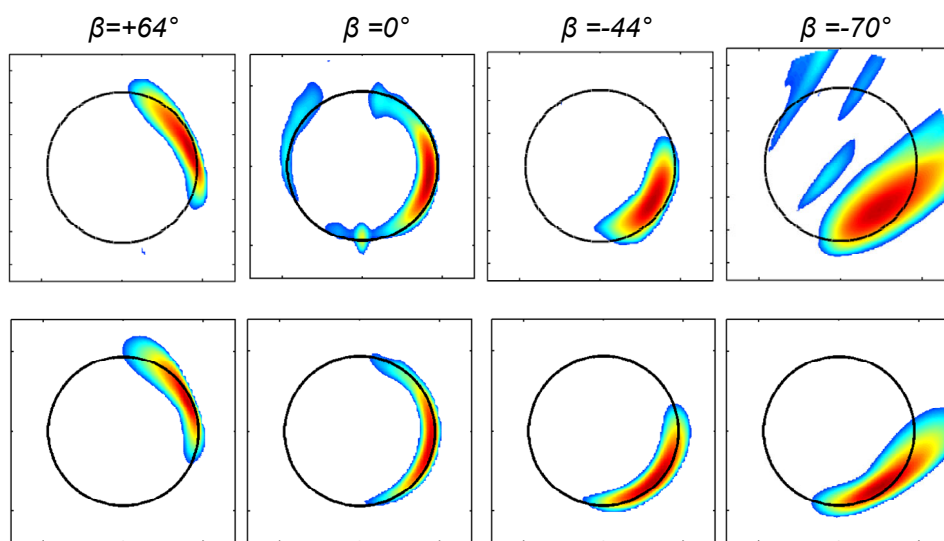


Figure 34 Measured (upper row) and predicted (lower row) source maps at different misalignment angles (800 Hz)

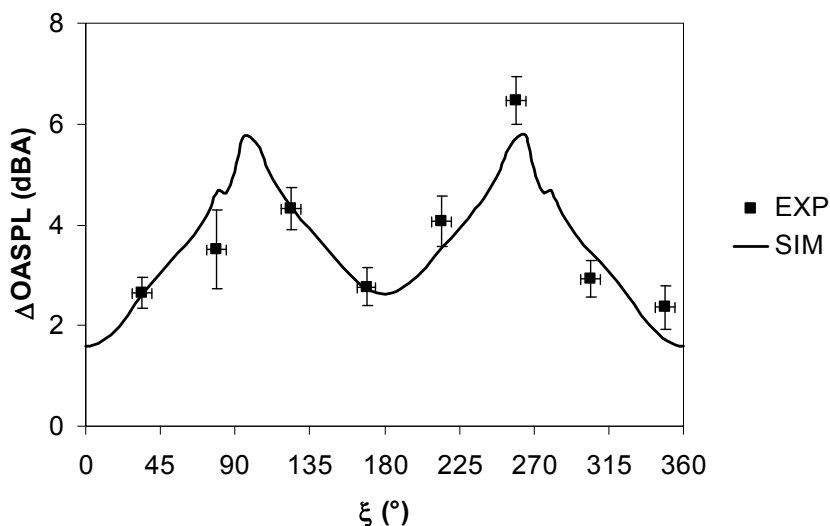


Figure 35 Measured and predicted swish amplitude as a function of far field position

Since the simulated source maps successfully reproduce the asymmetric source distribution found in the experiments, we expect that the variation in perceived sound level (swish) is also captured by the predictions. Figure 23 shows the variation in sound level for two measurement positions. From plots like these we can determine the (peak-to-trough) swish amplitude as a function of observer position. The experimental swish amplitudes for the eight ground microphones (Figure 31) are shown together with the predicted values in Figure 35. It can be seen that the swish amplitude is predicted within 1 dB for all directions. The highest swish is observed for microphones close to the rotor plane, where it can reach values of more than 6 dB.

In summary, the results in this section show that the characteristics of wind turbine noise can be well predicted using a semi-analytical, semi-empirical prediction method. Good agreement is obtained between prediction and experiment, not only in terms of source spectra and overall sound levels (as a function of rotor power), but also in terms of the noise source distribution in the rotor plane (as a function of frequency and observer position). Moreover, the turbine noise directivity and swish amplitude in different directions are accurately predicted. This allows us to apply the prediction method to calculate the noise at larger distances, which is the subject of the following section.

6.3 Prediction of noise and swish footprints

The prediction method is now applied to calculate time-dependent noise footprints of the 94-m diameter turbine shown in Figure 20, which is considered to be representative of a modern large wind turbine. Figure 36 shows instantaneous turbine noise footprints (top view) for four different rotor azimuth angles, up to a distance of ten times the rotor diameter. The turbine is located at the centre of the footprint, and the wind goes from left to right. The rotor azimuth at observer time is indicated in the upper right corner of each footprint. In order to limit the range of the dB scale, the levels are normalized using the horizontal distance to the turbine.

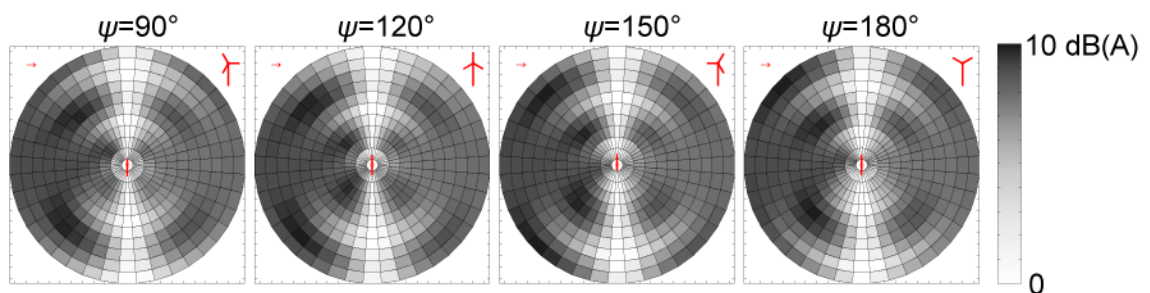


Figure 36 Predicted instantaneous noise footprints for increasing rotor azimuth angle. The wind goes from left to right

The footprints show two waves of increased sound level, one in each cross-wind direction, which start close to the turbine and propagate outward with the speed of sound. The wave to the

side of the descending blade is generated when the blade is at 1 o'clock, while the wave to the side of the ascending blade is generated when the blade is at 6 o'clock. Or, as mentioned before: you mainly hear the blade when it is coming towards you. After $\psi = 180^\circ$ the cycle repeats and both waves can be seen to propagate further to the edge of the footprints. The distance between two successive waves is about 5 rotor diameters, which is consistent with the time period of 1.33 s between the passage of two blades (the RPM is 15) and a speed of sound of 340 m/s.

Due to the passage of these sound waves from the blades, the noise levels in the crosswind directions vary significantly, while in the upwind and downwind directions the levels are quite constant at large distances. This is illustrated in Figure 37, which shows footprints of the average sound level (averaged over a complete revolution) and the swish (variation in sound level during a complete revolution). It can be seen that both footprints do not change significantly beyond a distance of a few rotor diameters. For both cross-wind directions, the *average* level is lower than in the upwind and downwind directions, but the *variation* in level is larger. Even at a large distance, trailing edge noise directivity and convective amplification may cause swish amplitudes up to more than 5 dB in the cross-wind directions. This may be an explanation for the 'Amplitude Modulation' phenomenon reported by many observers. Also note that at small distance to the turbine (about one rotor diameter) substantial swish is observed in *all* directions, which is consistent with the experimental results described above (Figure 35).

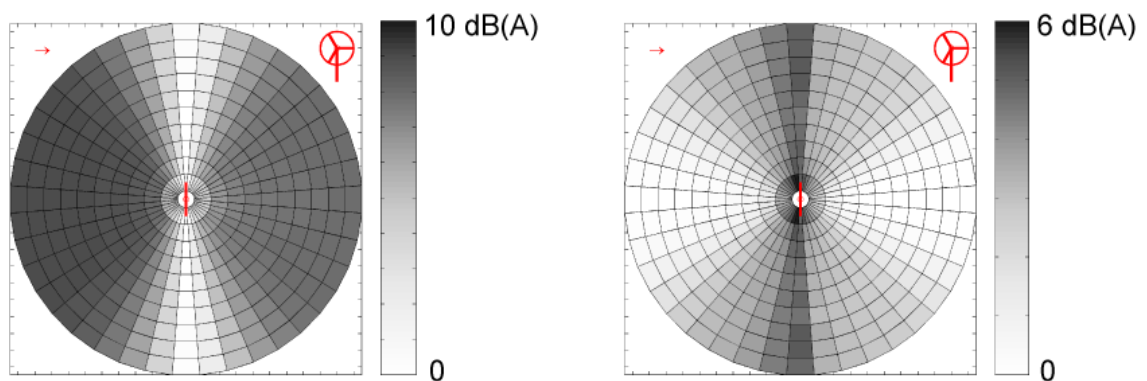


Figure 37 Predicted average footprint (left) and swish footprint (right) for a complete revolution

7 Reduction of wind turbine noise

In the preceding sections we have shown that trailing edge noise is the dominant noise source for typical modern wind turbines, and that we can predict the characteristics using a semi-analytical, semi-empirical method. In the present section we will address the question how we can *reduce* wind turbine noise. We will here focus on trailing edge noise; suggestions for reducing other sources (e.g. inflow turbulence noise or blunt trailing edge noise) can be obtained

from the characteristics described earlier in this chapter. A reduction in turbine noise can be exploited in several ways. First, it can prevent turbines from having to operate at reduced power during the night, due to noise constraints. Second, it enables us to erect more turbines on a given site, within the same overall noise limits. A noise reduction of 3 dB potentially doubles the number of turbines! Third, the distance to settlements can be reduced, so that more sites become available. Finally, quiet blade designs enable a larger rotor diameter and/or a higher RPM, thus increasing the energy yield for a given turbine. In this section we will describe a number of noise reduction concepts and discuss their performance in wind tunnel and field tests.

7.1 Reduction concepts

As mentioned before, trailing edge noise usually defines the lower bound of wind turbine noise. If all other potential noise sources are removed, trailing edge noise is what remains. In order to *further* reduce the noise from a wind turbine blade we should therefore reconsider Eq. (1), which describes how the trailing edge noise level depends on the different parameters. Since the sound scales with the fifth power of the flow speed, an obvious noise reduction technique is to lower the turbine RPM. In fact this 'low noise operation mode' is sometimes used to reduce sound emission from a turbine during the night. Theoretically, a 20% reduction in RPM already gives a noise reduction of 5 dB. However, the big disadvantage is that a reduction in RPM also reduces the power production. The same holds for an increase in blade pitch angle μ , which reduces the local angle of attack α (see Figure 3), yielding a smaller displacement thickness δ^* and as a result less noise. However, due to the reduced lift the power output is also reduced. Therefore, our objective will be to reduce trailing edge noise *without energy loss*.

One way to achieve a noise reduction without energy loss is to modify the airfoil shape such that the displacement thickness is reduced, while the aerodynamic performance is maintained [27]. The idea is schematically illustrated in Figure 38 (note that these are not the actual airfoil shapes). The sound from the reference airfoil is dominated by the low-frequency peak due to the suction side boundary layer. To reduce this peak, the optimized airfoil has less loading on the suction side, so that the suction side boundary layer thickness is reduced. As a result, the suction side peak has a lower level and higher frequency. In order to maintain the performance, the pressure side loading of the optimized airfoil is somewhat increased, which increases the pressure side boundary layer thickness. Nevertheless, the total sound level is reduced with respect to the reference airfoil. The optimized airfoil concept has been assessed using two-dimensional airfoil sections in small wind tunnels like the KAT (Figure 11), but also on a 4.5-m diameter model rotor in the larger DNW-LLF wind tunnel (Figure 39). Depending on the reference airfoil, average overall noise reductions of up to about 4 dB were obtained, without a significant degradation in aerodynamic performance. The assessment of this concept on a full-scale wind turbine will be discussed in the next section.

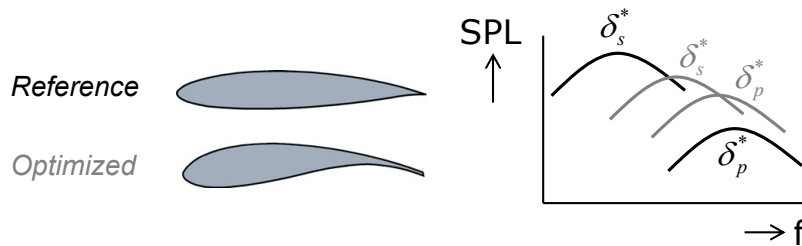


Figure 38 Reduction of trailing edge noise by modifying the boundary airfoil shape

Besides changing the flow parameters, we can also try to reduce noise by decreasing the acoustic radiation efficiency of the trailing edge. An example of this are the trailing edge serrations discussed before (Figure 9). By changing the angle γ between the path of the turbulent eddies and the normal to the trailing edge, the sound is scattered less effectively by the trailing edge. Serrations are intended to affect only the acoustic scattering at the trailing edge, and their aerodynamic effect should be small. Thus, the effects of an optimized airfoil shape and serrations are expected to supplement each other. The serration concept was investigated in a number of experimental studies on two-dimensional airfoils and model scale rotors. Typically, overall noise reductions of up to about 4 dB were achieved. In order to prevent excess high-frequency noise, it was found to be critical to align the plane of the serrations with the trailing edge flow (Figure 40). For a real turbine this may be complicated, since the trailing edge flow angle depends on the wind speed. The assessment of the serration concept on a full-scale wind turbine will be discussed in the next section.

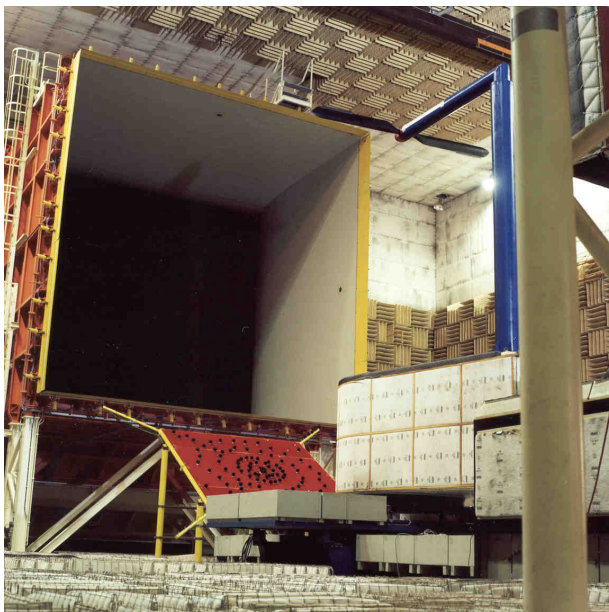


Figure 39 Model scale wind turbine (rotor diameter 4.5 m) in DNW-LLF wind tunnel

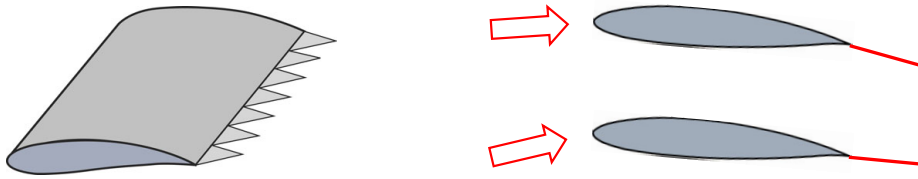


Figure 40 Alignment of serrations with trailing edge flow

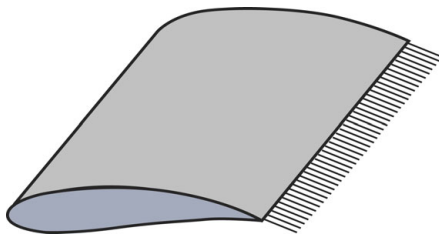


Figure 41 Trailing edge brushes

Another method to reduce the acoustic radiation efficiency is to add trailing edge brushes, which smooth the streamwise discontinuity at the trailing edge (Figure 41). This concept is inspired by the silent flight of the owl, which is attributed to the fluffy feathers at the trailing edge of its wings. Flexible brushes align automatically with the trailing edge flow and have shown significant noise reduction potential in wind tunnel tests on flat plates and two-dimensional airfoils [28]. However, the successful application of the brush concept on a full-scale wind turbine has not been reported yet.

7.2 Assessment of noise reduction concepts on a full-scale wind turbine

Two of the above-mentioned reduction concepts, the optimized airfoil shape and the trailing edge serrations, were tested on the 2.3 MW, 94-m diameter wind turbine shown in Figure 20. In order to compare the blade performance for identical weather and operation conditions, the rotor consisted of one standard (baseline) blade, one standard blade with trailing edge serrations, and one blade with an optimized airfoil shape. Since all the noise is produced by the outer part of the blades (Figure 25), only this part was modified. The optimized blade was nominally identical to the baseline blade, except for the outer ~30%, where it had a new airfoil. The serrated blade had the same nominal geometry as the baseline blade. The serrations were mounted to the outer 12.5 m of the blade (Figure 42). Their length was about 20% of the local chord, and varied as a function of radius. The plane of the serrations was aligned with the flow direction at the blade trailing edge (as determined from flow calculations). By aligning the serrations with the flow (at least for a certain wind speed range) it was attempted to minimize their aerodynamic impact and prevent increased high frequency noise by flow through the teeth.



Figure 42 Climber removing trips from serrated blade

From power and load measurements on the baseline and modified rotor, it was found that the in-plane and out-of-plane blade loads on the serrated blade (and, to a lesser extent, also on the optimized blade) were slightly higher than on the baseline blade, causing the aerodynamic performance of the modified blades to be similar or slightly better than the baseline blade. During the measurements on the baseline rotor, it was also verified that the sound produced by the three unmodified blades was practically the same: for the two blades used again in the present test campaign the difference was less than 0.05 dB.

In order to assess the differences in sound level between the three blades, we *could* use a single microphone to produce graphs like the one in Figure 23. However, this would not give us the complete picture, because it only shows the swish produced by each blade during a small part of the revolution. In reality each blade may produce noise during the complete revolution (as will be seen below). Therefore, more detailed acoustic measurements were carried out, using a large horizontal microphone array positioned about one rotor diameter upwind from the turbine (Figure 24). Using three rotating scan planes, the noise sources on the individual blades (averaged over many revolutions) could be localized and quantified (Figure 43). This figure shows that for low frequencies both modified blades are significantly quieter than the baseline blade, especially the serrated blade. For high frequencies however, both modified blades are

noisier than the baseline blade, especially the optimized blade. These trends are illustrated in Figure 45, which shows the integrated spectra for the three blades, averaged over all wind speeds between 6 m/s and 10 m/s (at 10 m height). These spectra confirm the low-frequency noise reduction and high-frequency noise increase for the modified blades.

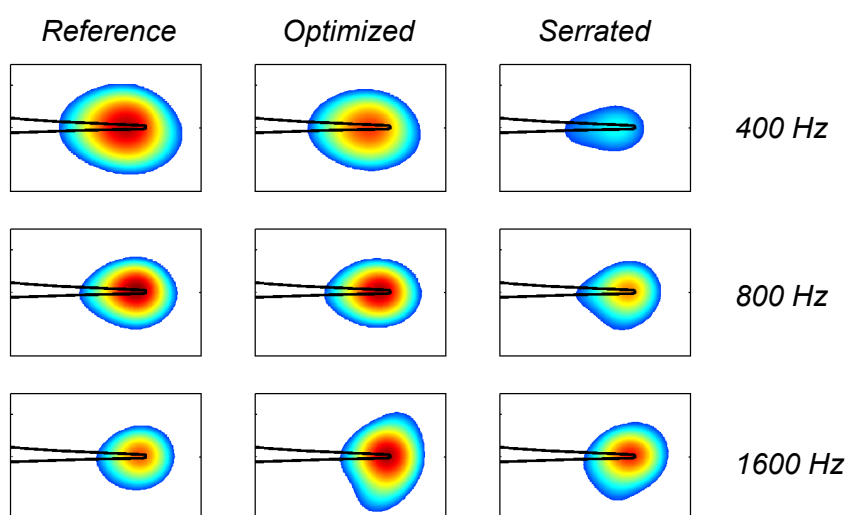


Figure 43 Acoustic source maps for baseline blade and two modified blades, averaged over all wind speeds. The black contour indicates the outer 32 m of the blade (trailing edge on upper side). The range of the dB scale is 12 dB

Since such a noise increase was not observed in the preceding two-dimensional wind tunnel tests, a more detailed analysis of the field results was carried out. This analysis showed that the noise increase at high frequencies is due to tip noise, which is mainly radiated during the upward part of the revolution. This is illustrated in Figure 44, which shows the dependence of the blade noise on rotor azimuth. The excess tip noise is found to be most important at low wind speeds, where the tip loading is high (Figure 46). This suggests that the tip noise is caused by the slightly higher blade loads on the modified blades, which may have led to a stronger tip vortex. As a result of the increased tip noise at low wind speeds, the overall noise reduction increases with increasing wind speed. Based on the spectra in Figure 45, *average* overall noise reductions of 0.5 dB and 3.2 dB are obtained for the optimized blade and the serrated blade, respectively. This 3 dB reduction demonstrates that wind turbine noise can be halved without adverse effects on the aerodynamic performance! Note that in this context 'halve' refers to the acoustic energy, i.e., two wind turbines *with* serrations would produce the same amount of noise as one turbine without serrations. It does *not* imply that the subjectively perceived loudness is reduced by 50% if a turbine is equipped with serrations. For this a noise reduction on the order of 10 dB would be required.

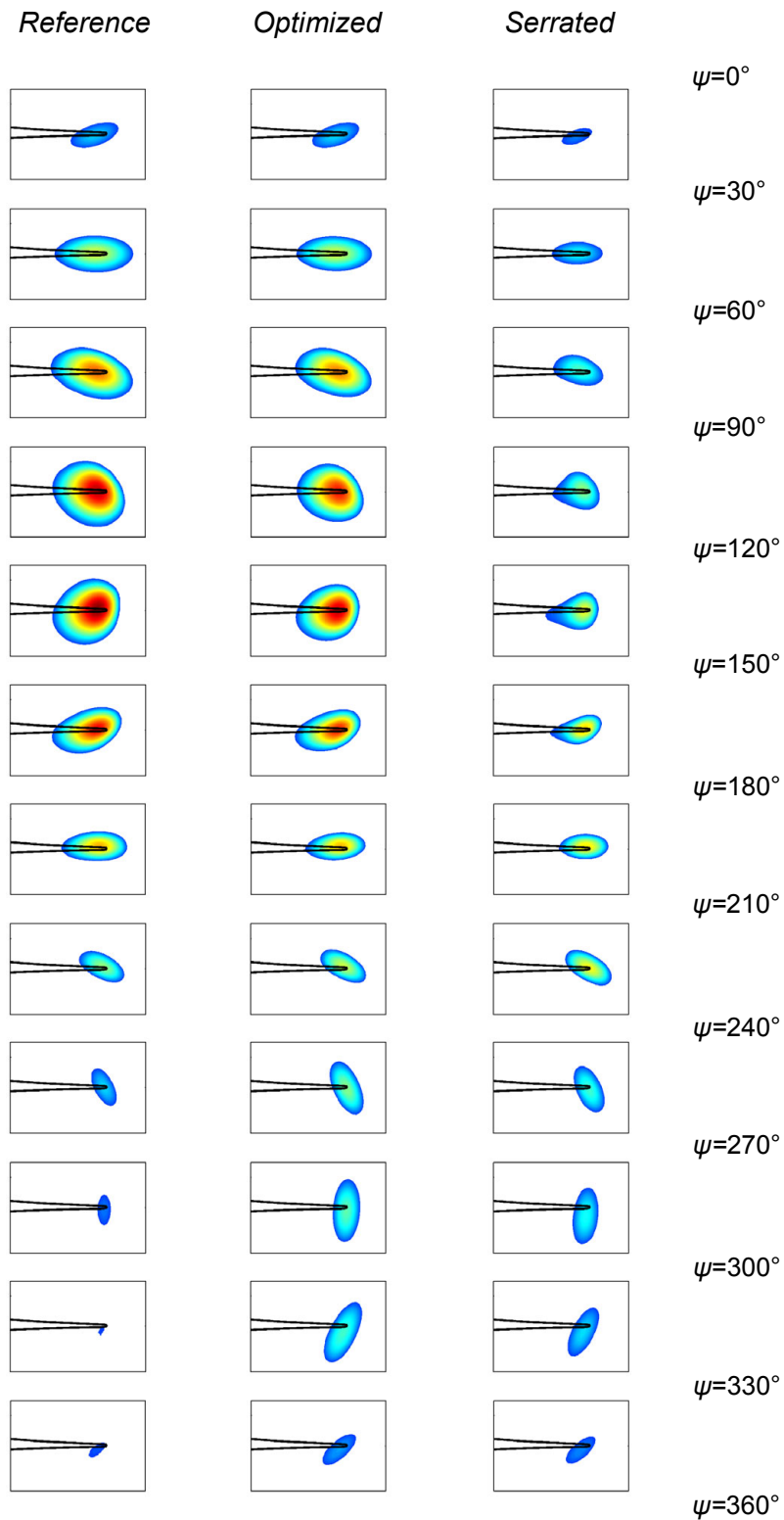


Figure 44 Dependence of blade noise on rotor azimuth ($\psi = 0^\circ$ corresponds to 12 o'clock). The maps are summed over all frequencies and averaged over all wind speeds. The range of the colour scale is 12 dB and the maximum is the same for all maps

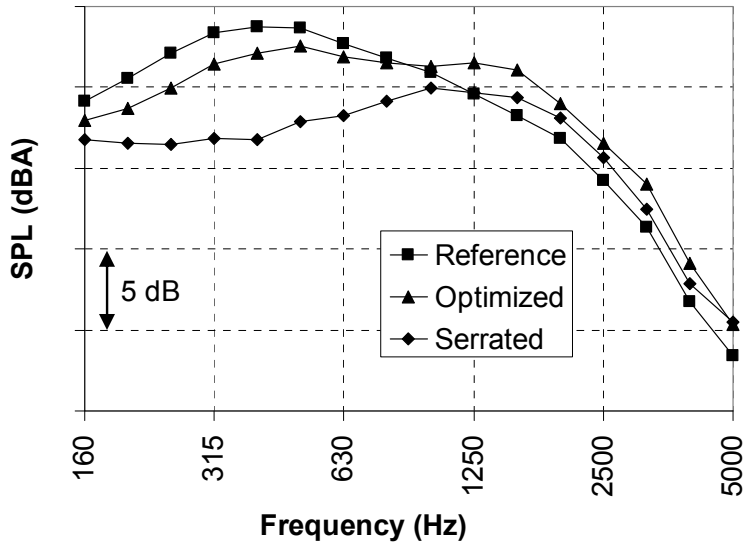


Figure 45 Integrated spectra for baseline blade and two modified blades, averaged over all wind speeds

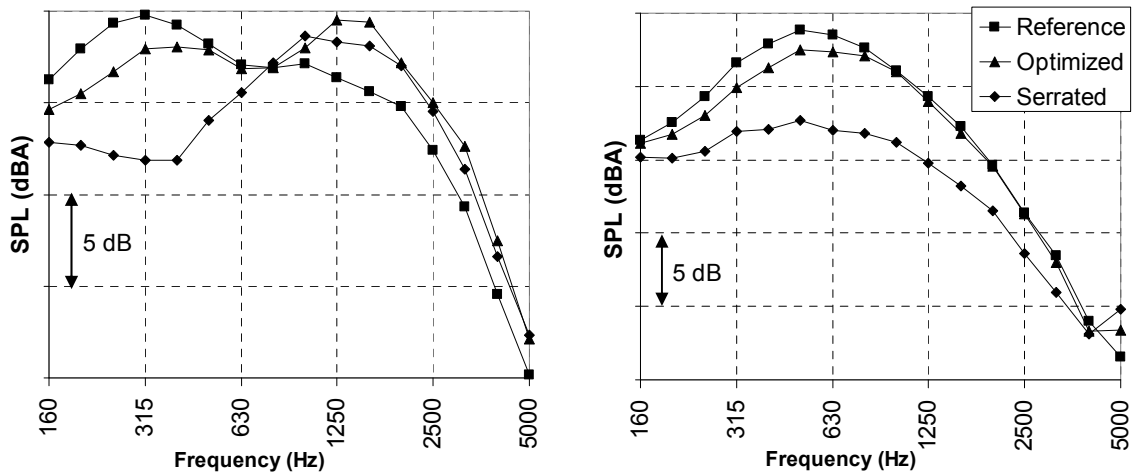


Figure 46 Integrated blade noise spectra at wind speeds of 7 m/s (left) and 10 m/s (right)

8 Conclusion

In this chapter we have addressed the primary sources of wind turbine noise. First, the different potential source mechanisms were described and the theoretical characteristics of flow-induced sound from wind turbine blades were explained. It was shown that the sound power scales with at least the 5th power of the flow speed, and that the directivity is generally not uniform.

Then, the noise sources on wind turbines were characterized experimentally by means of acoustic array measurements in the field. The test results indicated that the dominant noise

source for typical modern large wind turbines is broadband trailing edge noise from the outer part of the blades. The swishing character of the sound can be explained by trailing edge noise directivity and convective amplification: each time a blade moves towards the observer, a higher sound level is perceived.

Next, it was shown that a semi-analytical, semi-empirical prediction method can accurately predict the characteristics of wind turbine noise. Good agreement was found between predictions and experiment, not only in terms of sound levels and spectra, but also with regard to swish and turbine noise directivity. Calculated noise footprints show that swish amplitudes up to 5 dB can be expected for cross-wind directions, even at large distance.

Finally, different noise reduction concepts were described and two of them, an optimized airfoil shape and trailing edge serrations, were tested on a full-scale turbine. Both blade modifications yield a significant trailing edge noise reduction at low frequencies, but also exhibit increased tip noise at high frequencies. Nevertheless, the experimental results show that wind turbine noise can be halved by means of serrations, without adverse effects on the aerodynamic performance. In future, even larger reductions may be achieved using flexible trailing edge brushes.

References

- [1] F. van den Berg, E. Pedersen, J. Bouma, R. Bakker, WINDFARM perception: Visual and acoustic impact of wind turbine farms on residents - Final report, 2008.
- [2] E. Maris, P.J.M. Stallen, R. Vermunt, and H. Steensma, Noise within the social context: Annoyance reduction through fair procedures, *Journal of the Acoustical Society of America*, 121(4), pp 2000-2010, 2007.
- [3] S. Oerlemans, Detection of aeroacoustic sound sources on aircraft and wind turbines, PhD Thesis University of Twente, The Netherlands, 2009 (<http://doc.utwente.nl/67363/>). ISBN 978-90-806343-9-8. NLR Report NLR-TP-2009-511.
- [4] S. Wagner, R. Bareiss, and G. Guidati, *Wind Turbine Noise*, Springer, 1996.
- [5] H. Schlichting, *Boundary-Layer theory*, McGraw-Hill, 1979.
- [6] T.F. Brooks, D.S. Pope, and M.A. Marcolini, *Airfoil self-noise and prediction*, NASA Reference Publication 1218, 1989.
- [7] R. W. Paterson, R. K. Amiet, C. L. Munch, Isolated airfoil – tip vortex interaction noise, *AIAA paper 74-194*, 1974.
- [8] M. R. Fink, D. A. Bailey, *Airframe noise reduction studies and clean-airframe noise investigation*, NASA-CR-159311, 1980.
- [9] S. Moreau, M. Roger, J. Christophe, Flow features and self-noise of airfoils near stall or in stall, *AIAA paper 2009-3198*, 2009.
- [10] W.K. Blake, *Mechanics of Flow-Induced Sound and Vibration*, Volumes I and II, Academic Press, 1986.
- [11] J.E. Ffows Williams and L.H. Hall, Aerodynamic sound generation by turbulent flow in the vicinity of a scattering half plane, *Journal of Fluid Mechanics*, Vol. 40, part 4, 1970.
- [12] M.S. Howe, Noise produced by a sawtooth trailing edge, *The Journal of the Acoustic Society of America* 90, 1991.
- [13] R.K. Amiet, Noise due to turbulent flow past a trailing edge, *Journal of Sound and Vibration* 47, Vol. 3, 1976.
- [14] T. F. Brooks and T. H. Hodgeson, Trailing edge noise prediction using measured surface pressures, *Journal of Sound and Vibration* 78, 1981.
- [15] M. S. Howe, A review of the theory of trailing edge noise, *Journal of Sound and Vibration* 61, Vol. 3, 1978.
- [16] P. Migliore and S. Oerlemans, Wind tunnel aeroacoustic tests of six airfoils for use on small wind turbines, *Journal of Solar Energy Engineering* Vol. 126, 2004 (Chapter 7 of Ref. 3).
- [17] M. Herr, C. Appel, J. Dierke, R. Ewert, Trailing-Edge Noise Data Quality Assessment for CAA Validation, *AIAA paper 2010-3887*, 2010.

- [18] F. V. Hutcheson, T. F. Brooks, Effects of angle of attack and velocity on trailing edge noise, AIAA paper 2004-1031, 2004.
- [19] S. Moreau, M. Roger, Competing Broadband Noise Mechanisms in Low-Speed Axial Fans, AIAA Journal, Vol. 45, No. 1, 2007.
- [20] P. J. Moriarty, G. Guidati, P. G. Migliore, Recent improvement of a semi-empirical aeroacoustic prediction code for wind turbines, AIAA paper 2004-3041, 2004.
- [21] J. W. Slooff, W. B. de Wolf, H. M. M. van der Wal, J. E. J. Maseland, Aerodynamic and Aero-acoustic Effects of Flap Tip Fences, AIAA paper 2002-0848, 2002.
- [22] W. Dobrzynski, Almost 40 Years of Airframe Noise Research: What Did We Achieve?, Journal of Aircraft, Vol. 47, No. 2, 2010.
- [23] S. Oerlemans, P. Sijtsma, B. Méndez López, Location and quantification of noise sources on a wind turbine, Journal of Sound and Vibration 299, 869-883, 2007 (Chapter 5 of Ref. 3).
- [24] S. Oerlemans, M. Fisher, T. Maeder, K. Kögler, Reduction of wind turbine noise using optimized airfoils and trailing-edge serrations, AIAA Journal Vol. 47, No. 6, June 2009 (Chapter 8 of Ref. 3).
- [25] IEC norm 61400-11, Wind turbine generator systems – Acoustic noise measurement techniques, 2002.
- [26] S. Oerlemans, J. G. Schepers, Prediction of wind turbine noise and validation against experiment, International Journal of Aeroacoustics, Vol. 8, No. 6, 2009 (Chapter 6 of Ref. 3).
- [27] T. Lutz, A. Herrig, W. Würz, M. Kamruzzaman, E. Krämer, Design and wind tunnel verification of low noise airfoils for wind turbines, AIAA Journal, Vol 45, No. 4, 2007.
- [28] Herr, M., Design criteria for low-noise trailing edges, AIAA paper 2007-3470, 2007.



This page is intentionally left blank.

Appendix A Detection of sound sources using phased microphone arrays

This Appendix describes how sound sources can be localized and quantified using an array of microphones [3]. In order to provide an intuitive understanding of the technique, we will first give a qualitative description of delay-and-sum beamforming in the time domain. Then, we will see how the different sound sources in a source map can be quantified using a power integration method. Finally, some example applications will be presented, to illustrate the capabilities of acoustic arrays and to help interpretation of the wind turbine noise source maps in Chapter 2.

A.1 Beamforming

Consider a compact sound source in a homogeneous stagnant medium with sound speed c . The sound field is measured by an array of microphones (Figure 47). For simplicity a linear array is shown here, but the explanation is equally valid for a two-dimensional planar array. Due to the difference in distance r , the sound will arrive slightly earlier at microphone m_1 than at m_2 . Furthermore, since the pressure amplitude decreases with distance, the amplitude of the acoustic pressure p will be lower on m_2 than on m_1 . Now suppose we know the source is located in a specific plane (e.g. the wing of an aircraft or the rotor of a wind turbine), but the position *within* this plane is unknown. Then the source location can be determined on the basis of the measured signals as follows: first, a scan grid is defined in the plane where the source is expected. For each scan position, the microphone signals are shifted to account for the time the sound needs to travel from the scan position to the microphone. In addition, the amplitudes are adjusted to account for the distance between the scan position and the microphone. Next, the time-shifted, amplitude-adjusted signals from all microphones are summed. This procedure is called delay-and-sum.

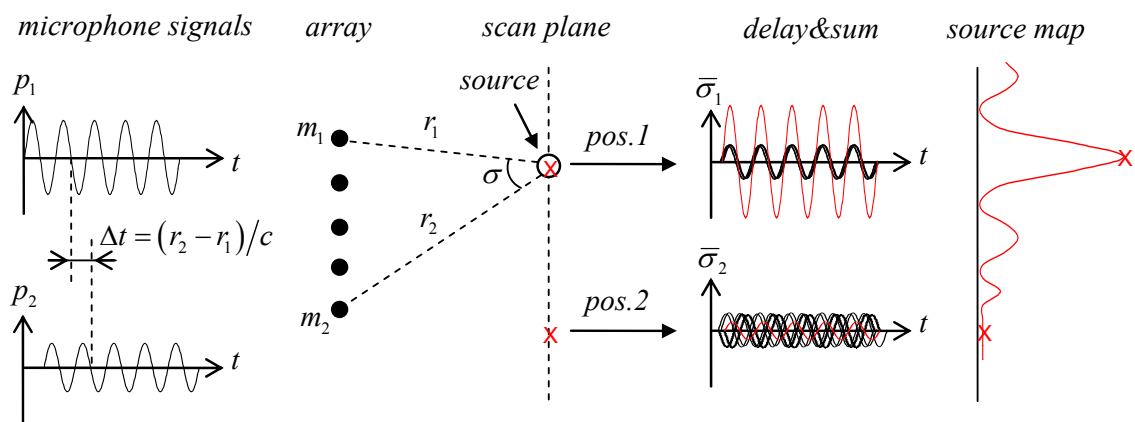


Figure 47 Delay-and-sum beamforming

If a sound source is present at a given scan position (position 1 in Figure 47), the shifted microphone signals will be in phase and their sum will have a high amplitude. If no source is present (position 2), the shifted signals will have random phase and the amplitude of their sum will be small. Thus, the phased array essentially amplifies the sound from the scan position (or focal point) with respect to sound from other directions. By plotting the (squared) amplitude as a function of scan position, a so-called *source map* is obtained. This source map shows peaks at the source locations. The strength of a source can be determined by dividing the reconstructed peak amplitude in the source map by the number of microphones. In the case of a planar array a two-dimensional source map is obtained and the amplitudes can be indicated by colours (Figure 48).

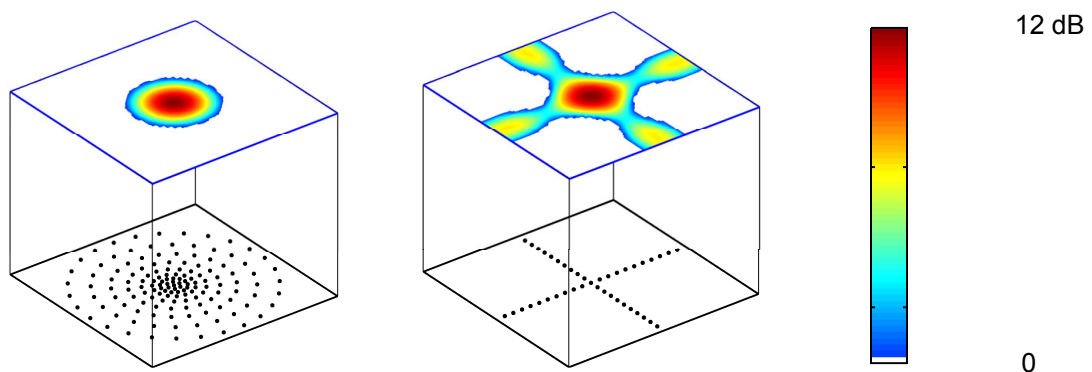


Figure 48 Simulated acoustic source maps of a 2 kHz point source for a random array (left) and a cross array (right). The size of the cube is 1 m^3

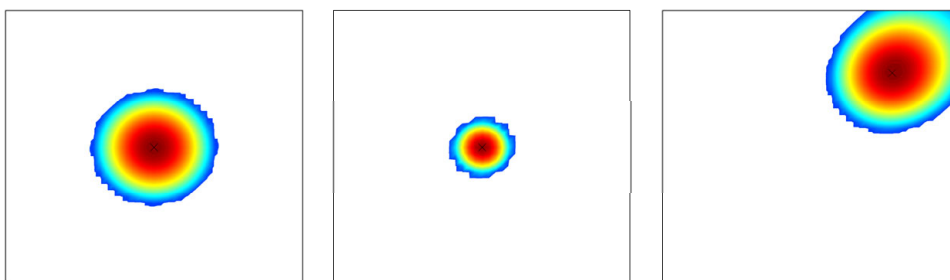


Figure 49 Simulated random-array source maps for 2 kHz (left), 4 kHz (middle), and for an oblique 2-kHz source (right)

The delay-and-sum technique illustrates several aspects of the beamforming methods used in this book. First, the main peak in the source map has a certain width, which determines the *resolution* of the array. In order to distinguish two different sources, their distance should be larger than the peak width at 3 dB below the peak level: the narrower the peak, the higher the resolution. The non-zero peak width can be understood if we consider a scan position just next to the actual source position. The time-shifted microphone signals for this position will still be partly in phase, resulting in a non-zero reconstructed amplitude. For a given scan position next

to the actual source, the phase error between the shifted signals will decrease with increasing wavelength, resulting in a higher reconstructed amplitude. Thus, the resolution of the array decreases with increasing wavelength, and therefore increases with frequency f (Figure 49). Similarly, it can be deduced that the resolution increases with the opening angle σ of the array, so that the peak width is roughly proportional to r/Df , where D is the size of the array. Note that the opening angle, and thus the effective array size, decreases when the source is not in front of the array. Thus, the array resolution decreases for oblique source directions (Figure 49).

Besides the main peak (or main lobe), the source map may also show *side lobes*, local maxima around the source position. These spurious sources are an inevitable consequence of the finite number of microphones in the array, and are difficult to distinguish from real secondary sources. Therefore, an important requirement of the array design is to keep the side lobe levels as low as possible. This can be achieved by the use of 'random arrays', in which the periodicity in microphone spacing is reduced (Figure 48).

In principle, multiple parallel scan planes (or any three-dimensional grid) can be used to estimate the distance to an unknown source. However, it should be noted that for a planar array the depth resolution (i.e., the resolution in the direction perpendicular to the array surface) is much lower than the lateral resolution. As a result, the three-dimensional main lobe of a point source has the shape of a cigar, with its long axis pointing to the array. In many cases this low depth resolution is actually an advantage, since the array results are rather insensitive to small deviations in distance (e.g. for curved wings or rotor blades).

Note that in the above explanation of the delay-and-sum technique no assumptions were made regarding the nature of the source. The method only requires that the pressure disturbance travels with the speed of sound, and that the pressure amplitude is inversely proportional to the distance. This is true for monopole-type sources in the free field, and in the acoustic far field also for dipoles and quadrupoles. If the source has a non-uniform directivity, the reconstructed source strength will be the average value over the solid angle covered by the array. Another requirement for beamforming is that the source radiates sound coherently in the direction of the array. The above explanation also shows that delay-and-sum beamforming is *not* an inverse method in the sense that a source distribution is 'sought' which matches the incoming sound field. The method simply performs an operation on the measured signals and involves no fitting or iterative procedures.

Delay-and-sum beamforming with a phased array is similar to source detection using parabolic or elliptic antennas. An elliptic mirror focuses the sound rays radiated from a potential source location to its focal point, where a microphone is placed. However, phased arrays have a number of important advantages. Whereas antennas must be physically steered to each scan position, so that many time-consuming measurements are needed to obtain a complete source map, a phased array only needs one measurement, and the scanning is done afterwards. The electronic processing also provides the flexibility to include e.g. flow effects, moving sources,

or spatial weighting of the microphone signals, whereas for an antenna the time delays and weighting are fixed because they are imposed by the geometry. Furthermore, phased array processing can be performed in the frequency domain, which allows the use of several special data analysis techniques.

A.2 Quantification of array results

In general we are not only interested in the source *locations*, but also in their *levels*. For well-resolved monopole sources the source level simply corresponds to the peak level in the acoustic source map. However, in practice this situation seldom occurs. Firstly, the main lobes from different sources may overlap or the source may be spatially extended (e.g. trailing edge noise). As a consequence, the peak levels in the source map depend on the extent of the source and on the (frequency-dependent) resolution of the array. Secondly, the array signals may suffer from coherence loss, which typically results in broader main lobes with a reduced level. Thirdly, the levels in the source map may be influenced by side lobes from other sources. To overcome these complications, a *power integration method* can be used. This technique sums the source powers in (part of) the measured source map, and corrects the result with a scaling factor obtained by performing a simulation for a monopole source at the centre of the integration region. The method is schematically explained in Figure 50. An integration contour is defined around the distributed source in the measured source map, and the integrated level is corrected using a (frequency-dependent) calibration function which is determined from a monopole simulation. The integration technique has been applied in many wind tunnel and field tests, and generally yields accurate relative source levels (i.e., differences between configurations). For certain conditions the *absolute* levels may be too low due to, for example, coherence loss effects.

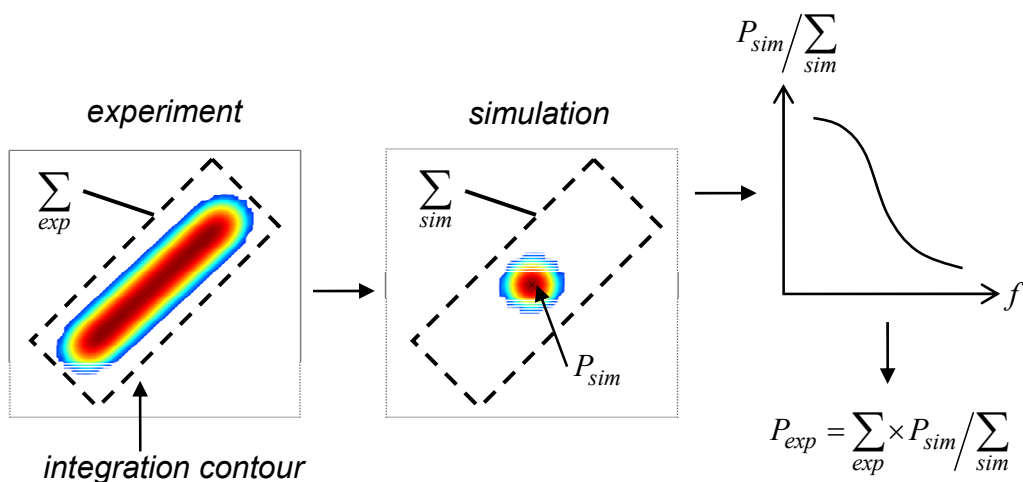


Figure 50 Source power integration method

A.3 Example applications

In this section some examples of acoustic array applications will be presented, to illustrate the capabilities and to help interpretation of the wind turbine noise source maps in Chapter 2. We will see several features that are also applicable to the wind turbine noise measurements, including (1) source localization for stationary and moving sources, (2) quantification of array results using the power integration method, and (3) application of the array technique in the wind tunnel and in the field.

Our first example is a (stationary) 1:10 scaled aircraft model in the 8x6 m² closed test section of the DNW-LLF wind tunnel (Figure 51). A 1-m diameter acoustic array was mounted flush in the wind tunnel floor. The resulting source maps show that for this particular configuration practically all wing noise is radiated from the leading edge slats.

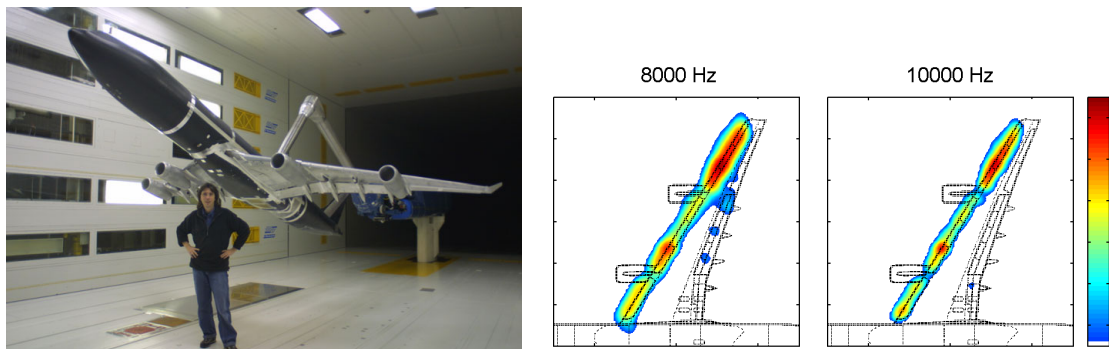


Figure 51 Aircraft model in DNW-LLF wind tunnel and corresponding source maps at model scale frequencies of 8 kHz and 10 kHz



Figure 52 Helicopter model in DNW-LLF wind tunnel, with (red) out-of-flow microphone array

Our second example is a helicopter model with main rotor and tail rotor in the open jet of the same DNW-LLF wind tunnel (Figure 52). In this case a $4 \times 4 \text{ m}^2$ out-of-flow microphone array was used. Even though the main and tail rotor blades are rotating, we can apply a stationary scan plane which coincides with the rotor plane. The resulting source maps (Figure 53) show that for this flight condition sound is radiated from both main and tail rotor, but that their relative importance depends on frequency. This is illustrated in the integrated spectra for both source areas, which confirm that the tail rotor is dominant at low frequencies, and the main rotor at high frequencies.

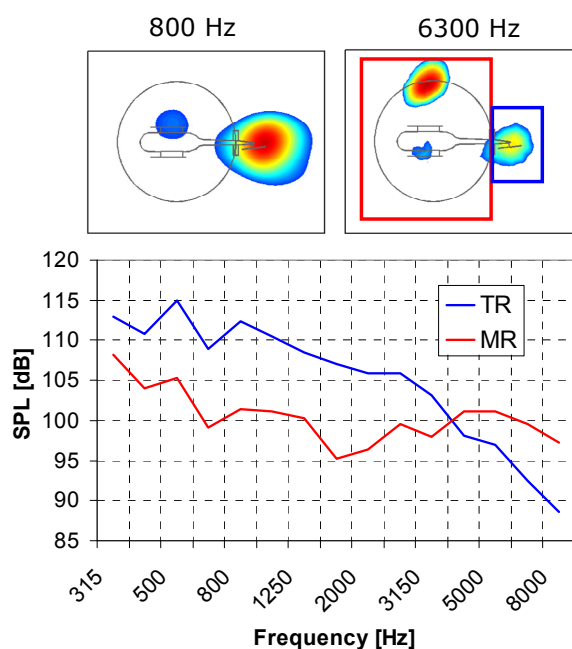


Figure 53 Source maps and integrated spectra for main rotor and tail rotor (level flight). The integration contours are shown in the 6.3 kHz source map

Figure 54 shows source maps for the same helicopter model, but now for the descent flight condition. The stationary source maps show that in this case most of the noise is generated by the main rotor, when the blades are on the retreating side. Now, using the same measurement data, we can also apply a scan plane which rotates along with the main rotor. The resulting 'rotating' source maps clearly show four equal spots, corresponding to the rotor blades. As expected, the four blades are equally noisy.

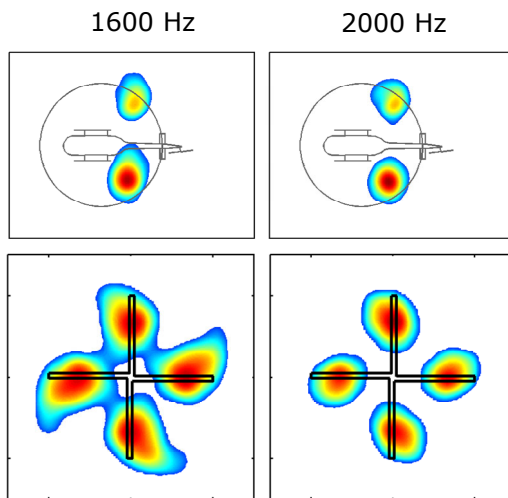


Figure 54 Stationary source maps (top) and corresponding rotating source maps (bottom) for descent flight

A final example is shown in Figure 55. This is a result of acoustic field measurements on landing aircraft at Amsterdam Airport. A 12-m diameter acoustic array, consisting of 243 microphones, was used. By employing a scan plane moving along with the landing aircraft, the different noise sources were localized. It can be seen that besides the engines, several airframe noise sources are present, including the slats, flaps, and landing gears.

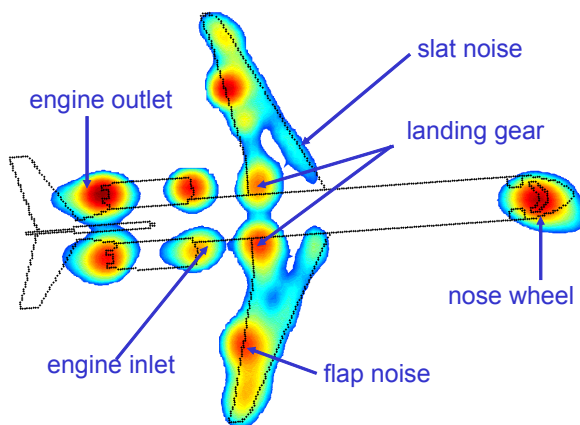


Figure 55 Acoustic source map for landing aircraft